International Geology Review
Publication details, including instructions for authors and subscription information:
http://www.tandfonline.com/loi/tigr20

Multistage metamorphism of garnet orthopyroxenites from the Maowu mafic-ultramafic complex, Dabieshan UHP terrane, eastern China

Yi Chen [a] , Kai Ye [a] , Shun Guo [a] , Teng-Fei Wu [a] & Jing-Bo Liu [a]
[a] State Key Laboratory of Lithospheric Evolution , Institute of Geology and Geophysics, Chinese Academy of Sciences , P.O. Box 9825 , Beijing , 100029 , China
Published online: 13 Mar 2013.

To cite this article: Yi Chen , Kai Ye , Shun Guo , Teng-Fei Wu & Jing-Bo Liu (2013) Multistage metamorphism of garnet orthopyroxenites from the Maowu mafic-ultramafic complex, Dabieshan UHP terrane, eastern China, International Geology Review, 55:10, 1239-1260, DOI: 10.1080/00206814.2013.772694

To link to this article: http://dx.doi.org/10.1080/00206814.2013.772694

International Geology Review, 2013
Vol. 55, No. 10, 1239–1260, http://dx.doi.org/10.1080/00206814.2013.772694

Taylor & Francis
Taylor & Francis Group

Multistage metamorphism of garnet orthopyroxenites from the Maowu mafic–ultramafic complex, Dabieshan UHP terrane, eastern China

Yi Chen*, Kai Ye, Shun Guo, Teng-Fei Wu and Jing-Bo Liu

State Key Laboratory of Lithospheric Evolution, Institute of Geology and Geophysics, Chinese Academy of Sciences, P.O. Box 9825, Beijing 100029, China

(*Accepted 30 January 2013*)

Garnet orthopyroxenites of the Maowu mafic–ultramafic body occur in coesite-bearing paragneisses in the Dabieshan ultrahigh-pressure (UHP) metamorphic complex. We have distinguished six stages of metamorphism based on integrated mineralogical–petrological investigations: M_1 – high-T/low-P metamorphism (~1.4 GPa, ~850°C); M_2 – low-T/low-P metamorphism (~1.4 GPa, ~750°C); M_3 – low-T/high-P metamorphism (2.1–2.5 GPa, 740–760°C); M_4 – UHP metamorphism (5.3–6.3 GPa, ~800°C); M_5 – early retrogression (<3 GPa, >750°C); M_6 – late retrogression (<2.3 GPa, <670°C). Detailed textures and mineral compositions indicate that the protolith of the Maowu garnet orthopyroxenites was a mantle refractory harzburgite or dunite that had been metasomatized by crust-derived silica-rich fluid or melt. M_1–M_2 defines an isobaric cooling P–T path, probably resulting from corner-flow in the mantle wedge above the subduction slab. M_2–M_4 defines an isothermal compressional P–T path, suggesting that the complex subsequently recycled into the deep upper mantle (up to ~200 km depth) and underwent HP–UHP metamorphism. M_4–M_6 defines a retrograde P–T path, implying that the rocks ascended to crustal levels attending exhumation of the UHP terrane, and was continuously metasomatized by fluid derived from the continent country rocks.

Keywords: Maowu mafic–ultramafic complex; garnet orthopyroxenite; multistage metamorphism; polyphase inclusions; P–T pseudosections

Introduction

The mantle association of orogenic garnet peridotites and garnet pyroxenites commonly occur in most high-pressure (HP) or ultrahigh-pressure (UHP) metamorphic belts resulting from continental collision, thickening, and foundering of continental material (e.g. Menzies *et al*. 2001; Medaris *et al*. 2005). These orogenic mantle rocks are commonly associated with eclogites and gneisses in UHP metamorphic terranes but preserve more complex metamorphic evidence than these UHP crustal rocks, some of them even preserve plenary metamorphic evidence from their mantle protolith to subsequent subduction and exhumation histories (e.g. Zhang *et al*. 2000; Yang and Powell 2008; Ye *et al*. 2009; Scambelluri *et al*. 2010). Although volumetrically minor, their geodynamic setting and UHP origin (>5 GPa) in some UHP terranes (Yang and Jahn 2000; Scambelluri *et al*. 2010) make orogenic mantle rocks an important window to the geodynamic processes of continental subduction, collision, exhumation, and crust–mantle interaction in a regional scare with global geodynamic implications.

The Maowu mafic–ultramafic complex hosted by garnet–coesite-bearing paragneisses is a typical orogenic peridotite body in the Dabieshan UHP terrane in eastern China (Figure 1). Even though several petrological and geochemical studies on this mafic–ultramafic complex have been reported (Okay 1994; Fan *et al*. 1996; Liou and Zhang 1998; Zhang *et al*. 1998; Jahn *et al*. 2003; Liu *et al*. 2006; Malaspina *et al*. 2006, 2009), most are focused on its geochemical characters, protolith origin, and UHP metamorphic ages. Many previous researchers have suggested that the protolith of the Maowu mafic–ultramafic complex originated from fractional crystallization of a mafic magma in the crustal level of the Yangtze Craton before the Triassic subduction (Okay 1994; Fan *et al*. 1996; Liou and Zhang 1998; Zhang *et al*. 1998; Jahn *et al*. 2003). Recently, Malaspina *et al*. (2006, 2009) suggested that the Maowu garnet pyroxenites originated from a refractory mantle harzburgite. Only Okay (1994) and Liou and Zhang (1998) have done petrological studies and they conclude that the Maowu garnet pyroxenites were subjected to three stages of metamorphism: (1) pre-peak

*Corresponding author. Email: chenyi@mail.iggcas.ac.cn

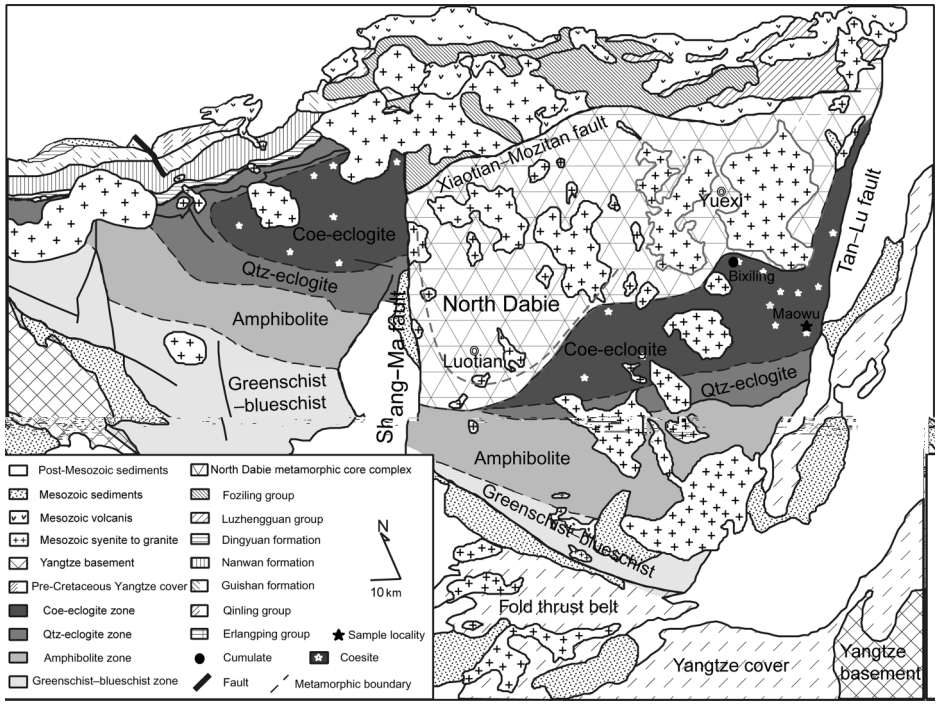

Figure 1. Geological sketch map of the Dabieshan Orogen in eastern China showing localities of the Maowu and Bixiling mafic–ultramafic body.

low-pressure granulite facies metamorphism (730 ± 30°C, 4 ± 2 kbar) characterized by the polyphase solid inclusions of orthopyroxene, amphibole, gedrite, chlorite, talc, phlogopite, sapphirine, corundum, and rutile; (2) peak UHP metamorphism (740 ± 50°C, 40 ± 10 kbar) recorded by the matrix garnet, pyroxene, Ti-chondrodite, and Ti-clinohumite; and (3) post-UHP amphibolite facies overprint (ca. 650°C, <15 kbar).

In this study, the metamorphic evolution of the Maowu garnet orthopyroxenite is reinvestigated, based on detailed mineralogical and petrological investigations. Our new data also suggest that the Maowu garnet orthopyroxenites were formed by metasomatic interactions between precursor mantle refractory harzburgite or dunite and slab-derived hydrous melt or fluid. Detailed textural and mineralogical evidence and thermodynamic modelling demonstrate that the Maowu garnet orthopyroxneites have preserved rare textural and mineralogical evidence of six stages of metamorphism related to the Triassic subduction and exhumation processes.

Geological setting

The Dabieshan UHP metamorphic terrane locates in the southwestern part of the Dabieshan–Sulu Orogen in eastern China (Figure 1). It was formed by subduction/collision of the Yangtze Craton beneath the Sino-Korean Craton in the Triassic (Li *et al*. 2000; Zheng *et al*. 2006). Several garnet peridotite and garnet–pyroxenite bodies occur as metre- to kilometre-sized blocks within the amphibolite-facies paragneisses in the Dabieshan–Sulu UHP terrane, and all of them suffered UHP metamorphism (Okay 1994; Zhang *et al*. 1998, 2000). The Maowu mafic–ultramafic body occurs in paragneisses in the Dabieshan UHP metamorphic terrane. It is a lens (50 m × 250 m) composed of millimetre- to centimetre-thick compositional layers, which are dominated by garnet orthopyroxenite and garnet-free orthopyroxenite with minor garnet clinopyroxenite, garnet websterite, harzburgite, and dunite. Rare eclogite lenses occur in the Maowu mafic–ultramafic body, thin omphacite veins (<2 cm) often occur in the garnet clinopyroxenite and garnet websterite layers. No lherzolite has been found. The boundaries between various rock types are generally sharp but not planar.

Many previous researchers have assumed that the protolith of the Maowu mafic–ultramafic body was a cumulate complex formed by fractional crystallization of a basaltic magma intruded into the crust of the Yangtze Craton, which experienced deep subduction and UHP metamorphism in the Triassic (Okay 1994; Fan *et al*. 1996; Liou and Zhang 1998; Zhang *et al*. 1998, 1999; Jahn *et al*. 2003). Malaspina *et al*. (2006, 2009) demonstrated that the Maowu garnet pyroxenites were formed by reactions between mantle wedge peridotite and silica-rich fluid or hydrous melt released from subduction crust. Bulk rock analyses show that all of the garnet orthopyroxenite,

garnet clinopyroxenite, garnet websterite, and garnet-free orthopyroxenite in the Maowu mafic–ultramafic body are enriched in light rare earth elements (LREE) and large ion lithophile elements (LILE) (Jahn *et al*. 2003; Malaspina *et al*. 2006). *In situ* LA-ICPMS analyses show that all of the poikilitic orthopyroxene grains in the Maowu pyroxenites have high nickel content (>2000 ppm) and are enriched in LREE and LILE (Malaspina *et al*. 2006, 2009), indicating that they are formed by interactions between olivine from a mantle harzburgite precursor and a silicon-rich hydrous melt sourced from the subduction crust at UHP conditions.

Petrography

To reveal the metamorphic evolution and mantle processes of the Maowu mafic–ultramafic body, we selected fresh garnet orthopyroxenite samples for detailed petrological study. Garnet orthopyroxenite is the dominant rock type in the Maowu mafic–ultramafic body. The studied garnet orthopyroxenite is mainly composed of garnet (~45%) and orthopyroxene (~45%) with minor clinopyroxene (1%), olivine (<1%), chromite (<1%), rutile (1%), Ti-clinohumite (1%), Ti-chondrodite (<1%), amphibole (<1%), chlorite (<1%), phlogopite (<1%), antigorite (<1%), and talc (<1%).

The garnet orthopyroxenite has a porphyroblastic texture. Coarse-grained garnet porphyroblasts (~5%, up to 1 cm) occur in the matrix of medium-grained (up to 2 mm) garnet, orthopyroxene, and clinopyroxene (Figure 2A). The matrix minerals show well-developed equilibrium granoblastic polygonal fabrics.

All garnet porphyroblasts record three stages of growth zones; each growth zone contains a distinct assemblage of mineral inclusions. The cores of the garnet porphyroblasts are 1–3 mm and contain abundant minute (20–100 μm) polyphase inclusions of sapphirine, garnet, corundum, spinel, pargasite, orthopyroxene, gedrite, rutile, talc, chlorite, phlogopite, apatite, and pyrite (Figures 2B–2E). The polyphase inclusions can be classified into two stages of mineral assemblages. One stage is a typical high-temperature mineral assemblage of sapphirine, corundum, spinel, pargasite, orthopyroxene, and garnet, they always occur in the centre parts of the polyphase inclusions (Figures 2B–2E); the later stage minerals are a typical low-temperature assemblage of chlorite, talc, gedrite, Ba–Cl amphibole, phlogopite, apatite, rutile, and pyrite, they always occur in the rim parts of the polyphase inclusions. The porphyroblastic garnets commonly have a thin (300–600 μm) mantle, which rarely contains fine-grained (10–20 μm) inclusions of orthopyroxene, pargasite, Cr-spinel, rutile, and chlorite (Figure 2A). No gedrite and talc have been found in the mantles of the garnet porphyroblasts. The rims of the garnet porphyroblasts are thin (<200 μm) and usually inclusion-poor (Figure 2A), rare rounded orthopyroxene, and chromite are observed in the rims of the garnet porphyroblasts. The rims of some porphyroblastic garnets are partially replaced by later stage kelyphite of amphibole, spinel, chlorite, and talc (Figure 5E).

Medium-grained (1–2 mm) garnet and orthopyroxene constitute the main matrix minerals (Figures 3A–3C). Rare medium-grained (1–2 mm) clinopyroxene and fine-grained (0.2–0.5 mm) Ti-chondrodite, Ti-clinohumite, rutile, chromite, and apatite also occur in the matrix (Figures 3A–3C). The cores of the matrix garnet commonly contain inclusions of orthopyroxene and rarely contain inclusions of pargasite, Cr-spinel, rutile, and chlorite (Figure 3D); however, no polyphase inclusions, such as those in the cores of the garnet porphyroblasts, have been found in the matrix garnet. The assemblage of mineral inclusions in the cores of the matrix garnet is similar to that of minerals included in the mantles of the garnet porphyroblasts. The rims of the matrix garnet rarely contain fine-grained (10–20 μm) inclusions of orthopyroxene, Ti-clinohumite, apatite, and chromite. The cores of matrix orthopyroxene commonly include fine-grained (50–200 μm) rounded garnet, Ti-clinohumite, Ti-chondrodite, chromite, apatite, and rarely include clinopyroxene; their rims are generally inclusion-free (Figures 3B and 3E). The garnet included in the cores of the matrix orthopyroxene also contains rounded orthopyroxene (Figure 3F). Very fine ilmenite and apatite rods are restricted in the cores of the matrix orthopyroxene. The matrix clinopyroxene contains inclusions of garnet, orthopyroxene, and rutile (Figure 3A). The matrix Ti-clinohumite and Ti-chondrodite are anhedral crystals and are in equilibrium with the matrix garnet and orthopyroxene (Figures 3B and 3C); their cores are rich in ilmenite rods (Figure 5D) and rarely contain rounded orthopyroxene and garnet (Figures 5A and 5B). The matrix Ti-clinohumite and Ti-chondrodite are commonly replaced by symplectite of very fine-grained ilmenite + olivine along their rims, fractures, and cleavages (Figures 5A–5E). The matrix apatite is anhedral and contains abundant monazite rods and rare orthopyroxene inclusions. Some rounded olivine (ol1) and orthopyroxene (opx1) inclusions occur rarely in the cores of the matrix orthopyroxene (opx2) (Figure 4). However, olivine never occurs in the matrix or as inclusions in the matrix garnet. This texture suggests that the matrix orthopyroxene might be formed by reaction products of former olivine and silicon-rich fluid (Malaspina *et al*. 2006, 2009).

The garnet orthopyroxenite exhibits two stages of weak decompressional retrogression. The early stage decompression is characterized by the replacement of the matrix Ti-chondrodite and Ti-clinohumite by vermicular symplectite of olivine + ilmenite along rims, fractures, and cleavages (Figures 5A–5E). In the symplectite domain,

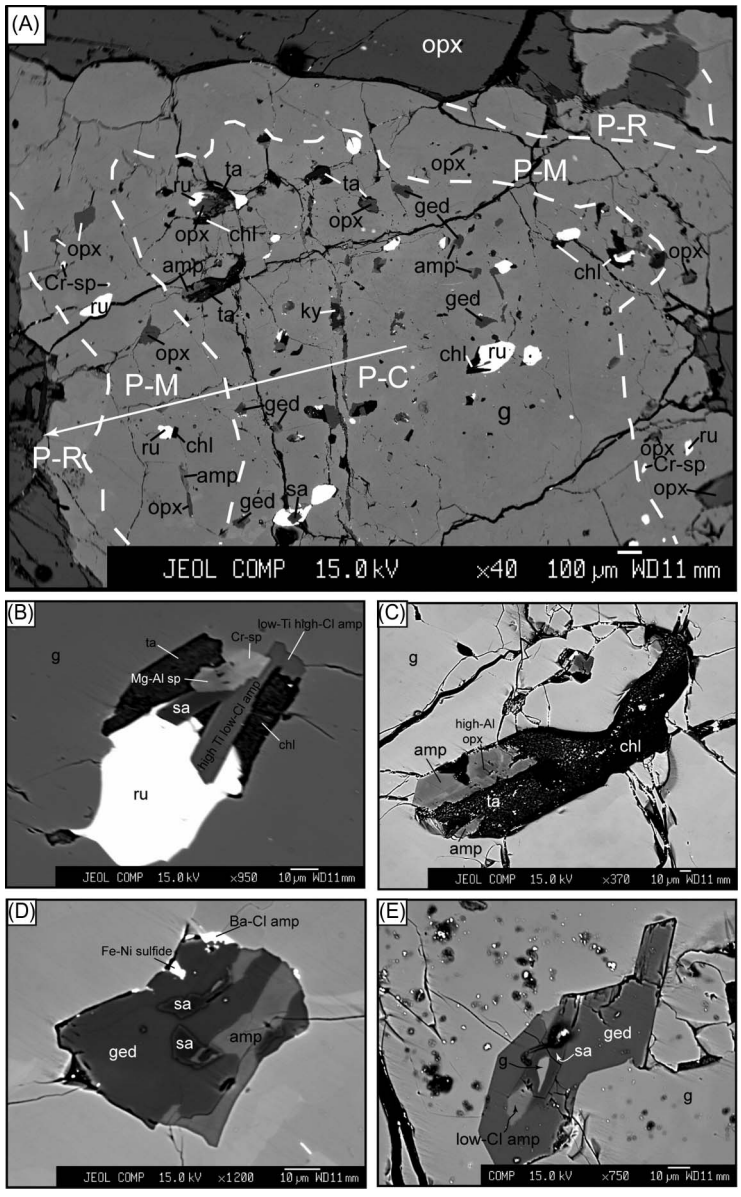

Figure 2. Back-scattered electron images showing textures of the porphyroblastic garnet and inclusions inside. (A) The core of the porphyroblastic garnet contains abundant polyphase inclusions, but rare inclusions in the mantle, and the rim is inclusion-free. (B) Back-scattered electron image showing polyphase inclusions of sapphirine, spinel, hornblende, rutile, talc, and chlorite in the core of the porphyroblastic garnet. Note that sapphirine, Mg–Al spinel, and high-Ti low-Cl hornblende occur in the centre of the inclusions, they are surrounded by chlorite, talc, Cr-spinel, and low-Ti high-Cl hornblende. (C) Polyphase inclusions of orthopyroxene, hornblende, chlorite, and talc in the core of the porphyroblastic garnet; high-Al orthopyroxene is surrounded by hornbenlde, talc, and chlorite. (D) Polyphase inclusions of sapphirine, amphibole, gedrite, and Fe–Ni sulphide in the core of the porphyroblastic garnet. (E) Polyphase inclusions of sapphirine, garnet, high-Ti low-Cl amphibole, and gedrite in the core of the porphyroblastic garnet. Note that tiny garnet and high-Ti low-Cl amphibole grains are included in sapphirine, which is surrounded by gedrite.

later stage kelyphite of chlorite and magnetite usually cut the symplectite into fragments (Figure 5B). Rims of garnets are occasionally replaced by fine-grained kelyphites of amphibole, spinel, chlorite, and talc (Figure 5E); rims of the matrix orthopyroxene are occasionally replaced by kelyphites of chlorite, talc, magnetite, phlogopite, and antigorite (Figure 5F).

Mineral chemistry

Mineral compositions were analysed using a JEOL 8100 microprobe analyser in the State Key Laboratory of Lithospheric Evolution, Institute of Geology and Geophysics, Chinese Academy of Sciences. Analytical conditions were 15 kV accelerating voltage, 20 nA beam current, and 20 s counting time. Representative

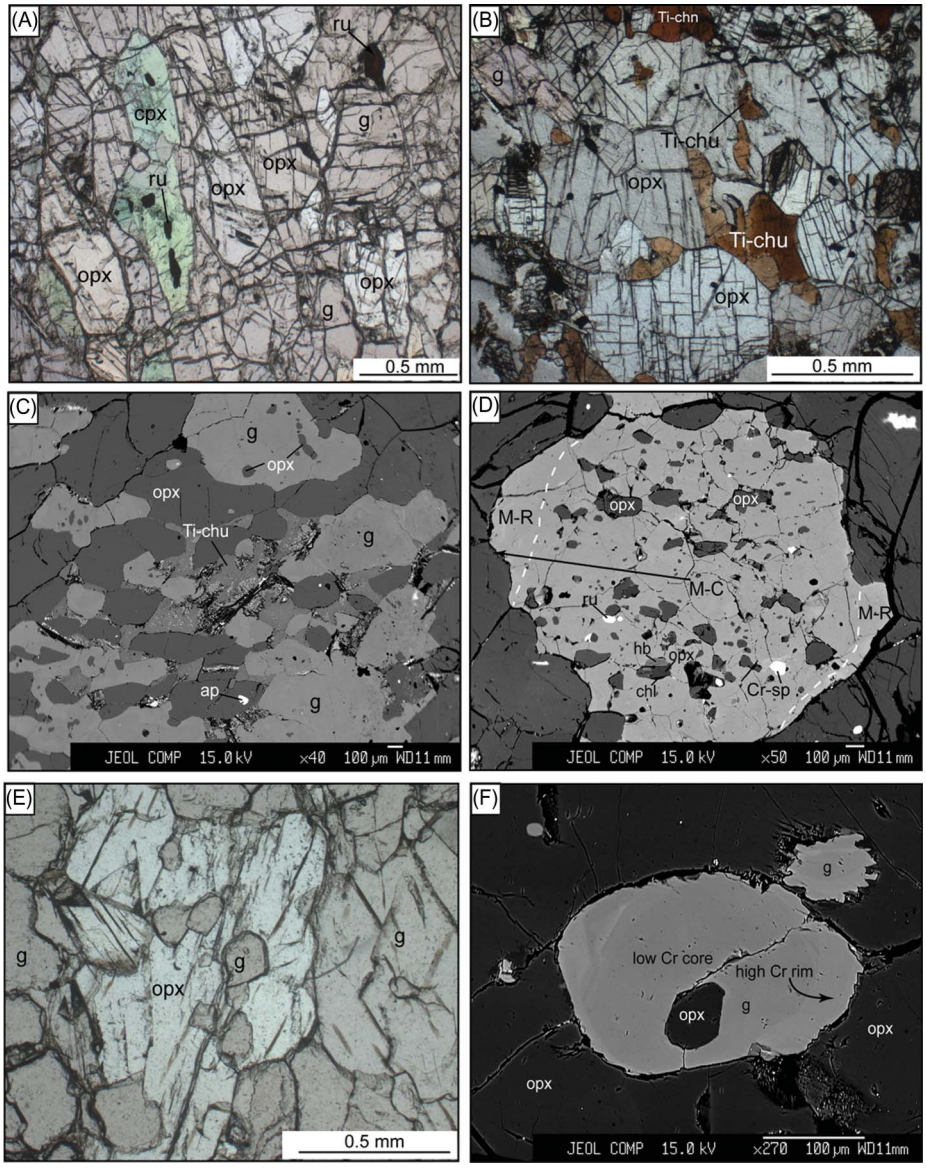

Figure 3. (A) Photomicrograph showing matrix garnet, orthopyroxene, and clinopyroxene; rutile commonly occurs as inclusions in the clinopyroxene. (B) Photomicrograph showing matrix orthopyroxene, Ti-chondrodite, Ti-clinohumite, and garnet; Ti-clinohumite also occurs as inclusions in the orthopyroxene. (C) Back-scattered electron image showing matrix garnet, orthopyroxene, and Ti-clinohumite. (D) Back-scattered electron image showing abundant inclusions of orthopyroxene, pagasitic amphibole, Cr-spinel, rutile, and chlorite in the core of the matrix garnet. (E) Photomicrograph showing rounded garnet inclusions in the core of the matrix orthopyrxoxene. (F) Back-scattered electron image showing rounded garnet inclusions in the core of the matrix orthopyrxoxene; the garnet inclusion is zoned with dark low-Cr core and bright high-Cr rim, its core contains rounded orthopyroxene inclusion.

compositions of garnet, orthopyroxene, clinopyroxene, olivine, spinellide, Ti-clinohumite, Ti-chondrodite, and amphibole are listed in Tables 1–5, respectively.

Garnet

Four textural types of garnet were observed, each textural type of garnet has very constant composition; however, different textural types of garnet exhibit significant but distinctive variations in composition.

(1) The tiny garnets included in the sapphirine in the polyphase inclusions contain higher MgO (20.32–20.67 wt.%) and lower CaO (1.84–2.13 wt.%) relative to the cores of garnet porphyroblasts (Table 1).

(2) Porphyroblastic garnets commonly display three stages of growth zones (Figure 6A). The inclusion-rich cores (approximately 2 mm, P-C) of the porphyroblastic garnet are homogeneous, they contain very low Cr_2O_3 (0.01–0.05 wt.%)

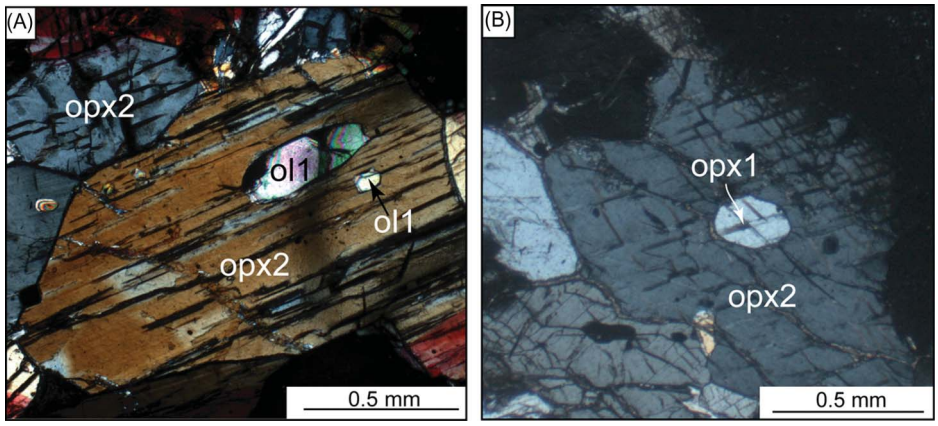

Figure 4. Photomicrographs showing fine-grained protolith olivine (ol1) (A) and orthopyroxene (opx1) (B) in the cores of the matrix orthopyroxene (opx2).

Table 1. Representative compositions of garnet, formula unit based on 12 oxygen.

Sample no.	06MW11	06MW11	06MW11	06MW11	06MW11	06MW11	06MW11	06MW11	06MW11	06MW11
Analysis no.	298	44	169	170	172	176	223	87	189	191
Texture	Incl. in sa	P-C	P-M	P-IR	P-OR	M-C	M-IR	M-OR	Incl.-C	Incl.-R
SiO_2	41.97	42.16	41.91	42.13	41.65	41.97	41.62	41.77	41.83	41.76
TiO_2	0.08	0.00	0.03	0.03	0.06	0.00	0.00	0.00	0.00	0.05
Al_2O_3	23.28	23.60	23.19	22.45	22.41	23.33	22.44	22.88	23.26	22.67
Cr_2O_3	0.04	0.04	0.06	1.27	0.44	0.06	1.36	0.31	0.12	1.22
FeO	10.84	11.86	11.23	11.67	11.68	11.34	11.45	11.47	11.30	11.59
MnO	0.28	0.37	0.45	0.39	0.36	0.30	0.43	0.37	0.38	0.41
MgO	20.67	19.41	20.02	19.92	19.89	19.81	19.68	19.46	19.78	19.65
CaO	2.13	3.25	2.53	2.60	2.69	2.84	2.59	2.84	2.85	2.59
Na_2O	0.01	0.04	0.00	0.01	0.03	0.01	0.00	0.03	0.00	0.00
K_2O	0.00	0.01	0.00	0.00	0.01	0.02	0.04	0.00	0.00	0.00
NiO	0.03	0.00	0.00	0.01	0.02	0.01	0.03	0.00	0.00	0.00
Total	99.32	100.72	99.42	100.48	99.23	99.70	99.64	99.12	99.52	99.93
Si	3.000	2.992	3.003	3.004	2.998	3.001	2.993	3.003	2.998	2.994
Ti	0.004	0.000	0.002	0.002	0.003	0.000	0.000	0.000	0.000	0.003
Al	1.961	1.982	1.958	1.886	1.901	1.966	1.902	1.938	1.964	1.916
Cr	0.002	0.002	0.003	0.072	0.025	0.003	0.077	0.017	0.007	0.069
Fe	0.648	0.704	0.673	0.696	0.703	0.678	0.688	0.689	0.677	0.695
Mn	0.017	0.022	0.027	0.023	0.022	0.018	0.026	0.023	0.023	0.025
Mg	2.203	2.054	2.139	2.117	2.135	2.112	2.109	2.107	2.113	2.100
Ca	0.163	0.247	0.194	0.199	0.208	0.217	0.199	0.219	0.219	0.199
Na	0.001	0.005	0.000	0.002	0.004	0.002	0.000	0.004	0.000	0.000
K	0.000	0.001	0.000	0.000	0.001	0.002	0.004	0.000	0.000	0.000
Ni	0.002	0.000	0.000	0.000	0.001	0.000	0.002	0.000	0.000	0.000
X_{Mg}	0.773	0.745	0.761	0.753	0.752	0.757	0.754	0.753	0.757	0.751
Uv	0.1	0.1	0.2	3.7	1.3	0.2	3.9	0.9	0.3	3.5
Alm	25.2	23.2	22.2	22.1	22.6	22.4	21.9	22.5	22.3	22.2
Prp	68.8	67.8	70.4	67.2	68.7	69.7	67.0	68.7	69.5	67.2
Grs	5.3	8.1	6.4	6.3	6.7	7.2	6.3	7.1	7.2	6.4
Sps	0.5	0.7	0.9	0.7	0.7	0.6	0.8	0.7	0.8	0.8

Notes: P-C, core of porphyroblastic garnet; P-M, mantle of porphyroblastic garnet; P-IR, inner rim of porphyroblastic garnet; P-OR, outer rim of porphyroblastic garnet; M-C, core of matrix garnet; M-IR, inner rim of matrix garnet; M-OR, outer rim of matrix garnet; Incl.-C, core of garnet inclusion in the core of matrix orthopyroxene; Incl.-R, rim of garnet inclusion in the core of matrix orthopyroxene; Uv, uvarovite; Alm, almadine; Prp, pyrope; Grs, grossular; Sps, spessatine.

and MgO (19.12–19.73 wt.%), with high CaO (2.91–3.76 wt.%) and FeO (11.70–12.82 wt.%). The narrow mantles (approximately 500 μm, P-M) of porphyroblastic garnet contain higher MgO (19.75–20.81 wt.%), and lower CaO (2.33–2.84 wt.%) and FeO (11.15–11.62 wt.%). The inner rims (approximately 100 μm, P-IR) contain the highest Cr_2O_3 (1.16–1.54 wt.%); their

Table 2. Representative compositions of orthopyroxene, clinopyroxene, and olivine.

Sample no.	06MW11	06MW11	06MW11	06MW11	06MW11	06MW11	06MW11	06MW11	06MW11	06MW11	06MW11	06MW14	06MW13	06MW11	06MW11
Analysis no.	139	150	260	200	51	171	181	215	298	127	128	129	64	123	38
Mineral	opx	opx	opx	opx	opx	opx	opx	opx	opx	cpx	cpx	cpx	ol	ol	ol
Texture	In amp in g P-C	Incl. in g P-C	Incl. in g P-M	Incl. in g M-C	M-C	Incl. in g P-R	Incl. in g M-R	M-R	opx in opx M-C	M-C	M-R	cpx in opx M-C	ol in opx M-C	sym. after Ti-chu	sym. after Ti-chn
SiO_2	56.11	57.43	57.56	56.81	57.81	57.75	57.69	57.37	57.51	55.06	55.52	55.28	41.07	40.97	40.51
TiO_2	0.01	0.02	0.00	0.07	0.00	0.00	0.00	0.02	0.02	0.02	0.00	0.02	0.00	0.12	0.09
Al_2O_3	3.70	0.89	0.58	0.51	0.06	0.09	0.08	0.18	0.06	1.40	1.20	0.94	0.00	0.00	0.00
Cr_2O_3	0.03	0.02	0.01	0.05	0.02	0.00	0.00	0.07	0.04	1.08	0.96	1.10	0.00	0.01	0.04
FeO	6.64	5.99	5.40	5.34	4.98	5.01	5.02	5.31	4.64	1.87	2.01	1.95	7.73	6.60	7.23
MnO	0.02	0.05	0.10	0.08	0.06	0.09	0.00	0.07	0.06	0.05	0.04	0.06	0.10	0.06	0.09
MgO	34.13	35.54	36.08	35.86	35.72	36.13	35.92	36.09	36.82	16.09	16.40	16.93	50.01	50.31	50.72
CaO	0.04	0.05	0.07	0.04	0.06	0.07	0.05	0.07	0.07	23.86	23.23	23.43	0.04	0.00	0.01
Na_2O	0.00	0.01	0.00	0.00	0.01	0.00	0.00	0.00	0.00	1.37	1.20	1.28	0.00	0.02	0.00
K_2O	0.02	0.00	0.00	0.00	0.00	0.03	0.00	0.01	0.00	0.03	0.01	0.02	0.00	0.01	0.00
NiO	0.12	0.13	0.14	0.26	0.25	0.28	0.24	0.24	0.02	0.15	0.18	0.22	0.41	0.96	0.59
Total	100.82	100.13	99.94	99.01	99.57	99.43	99.00	99.43	99.23	100.98	100.75	101.22	99.36	99.06	99.28
O	6	6	6	6	6	6	6	6	6	6	6	6	4	4	4
Si	1.961	1.968	1.971	1.963	1.999	1.986	1.993	1.974	1.974	1.975	1.997	1.975	1.005	0.996	0.990
Ti	0.000	0.000	0.000	0.002	0.000	0.000	0.000	0.000	0.001	0.001	0.000	0.000	0.000	0.004	0.002
Al	0.140	0.036	0.023	0.021	0.002	0.004	0.003	0.007	0.003	0.059	0.051	0.040	0.000	0.000	0.000
Cr	0.001	0.000	0.000	0.001	0.001	0.000	0.000	0.002	0.001	0.031	0.027	0.031	0.000	0.001	0.001
Fe	0.192	0.172	0.154	0.154	0.144	0.144	0.145	0.153	0.133	0.056	0.061	0.058	0.158	0.125	0.147
Mn	0.001	0.002	0.003	0.002	0.002	0.003	0.000	0.002	0.002	0.001	0.001	0.002	0.002	0.002	0.002
Mg	1.756	1.816	1.842	1.848	1.842	1.852	1.850	1.851	1.884	0.860	0.879	0.902	1.825	1.855	1.847
Ca	0.001	0.002	0.003	0.001	0.002	0.002	0.002	0.002	0.002	0.917	0.895	0.897	0.001	0.000	0.000
Na	0.000	0.000	0.000	0.000	0.001	0.000	0.000	0.000	0.000	0.095	0.084	0.089	0.000	0.000	0.000
K	0.001	0.000	0.000	0.000	0.000	0.001	0.000	0.000	0.000	0.001	0.000	0.001	0.000	0.000	0.000
Ni	0.003	0.004	0.004	0.007	0.007	0.008	0.007	0.007	0.001	0.004	0.005	0.006	0.008	0.017	0.012
X_{Mg}	0.902	0.914	0.923	0.923	0.927	0.928	0.927	0.924	0.934	0.939	0.936	0.939	0.920	0.937	0.926

Notes: P-C, porphyroblaste core; P-M, porphyroblaste mantle; P-R, porphyroblaste rim; M-C, matrix core; M-R, matrix rim; Incl., inclusion; sym., symplectite.

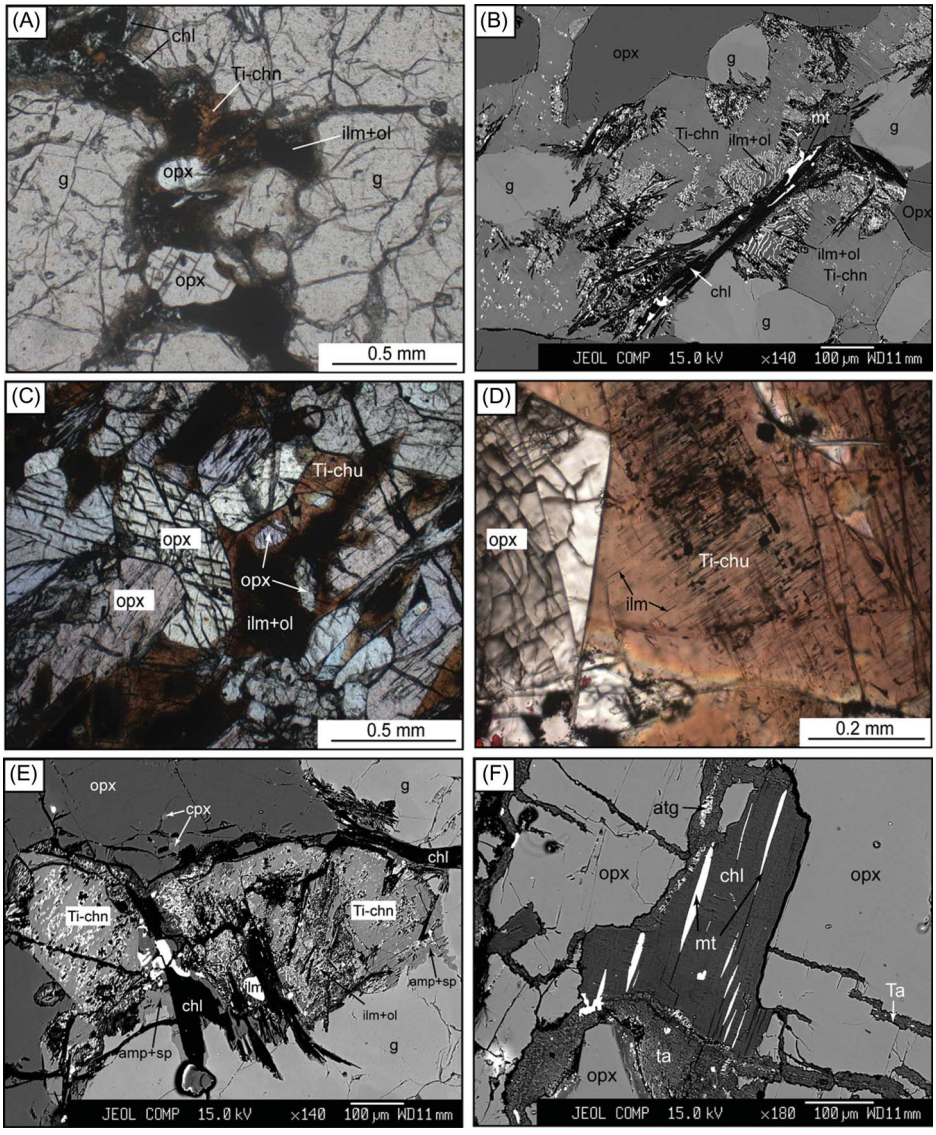

Figure 5. Photomicrographs (A, C, and D) and back-scattered electron images (B, E, and F) showing retrograde textures in the garnet orthopyroxenite. (A) Rim of the matrix Ti-chondrodite is replaced by fine-grained black symplectite of ol + ilm. (B) Rim of the matrix Ti-chondrodite is replaced by fine-grained symplectite of ol + ilm; later stage kelyphite of chlorite and magnetite cut the symplectite of ol + ilm and garnet into fragments. (C) Rim of the matrix Ti-clinohumite is replaced by fine-grained symplectite of ol + ilm. (D) Ilmenite rods in the core of Ti-clinohumite. (E) Rim of matrix garnet is replaced by fine-grained kelyphite of amphibole, chlorite, and spinel. (F) Rim of matrix orthopyroxene is replaced by chlorite, talc, antigorite, and magnetite.

MgO content is slightly lower and FeO content is slightly higher than those of their mantles (Figure 6A). The outer rims (50 μm, P-OR) show a retrograde zoning, their Cr_2O_3 and MgO contents decrease gradually, which are compensated by the increase of Al_2O_3 and FeO contents (Figure 6A).

(3) The medium-grained matrix garnets are also chemically zoned (Table 1, Figure 6B). Their cores (M-C) contain very low Cr_2O_3 (0.03–0.08 wt.%) and high Al_2O_3 (23.12–23.85 wt.%), which are similar to the compositions of the mantles of garnet porphyroblasts (Figure 6). The inner rims of the matrix garnet (M-IR) contain higher Cr_2O_3 and lower Al_2O_3 relative to their cores, they have the same composition as the inner rims of garnet porphyroblasts. Similar to the outer rims of the garnet porphyroblasts, the outer rims of the matrix garnet also show a retrograde zone, their Cr_2O_3 content decreases gradually, which is compensated by the increasing of Al_2O_3 content (Figure 6B, Table 1).

Table 3. Representative compositions of spinellide, formula unit based on 4 oxygen.

Sample no.	06MW11	06MW11	06MW11	06MW11	06MW11	06MW11	06MW11	06MW11
Analysis no.	48	162	183	56	277	75	57	155
Texture	With sa in g P-C	With chl in g P-C	Incl. in g P-M	Incl. in g M-C	Incl. in opx M-C	Incl. in g P-R	Incl. in g M-R	Kely. after g
SiO_2	0.07	0.00	0.02	0.08	0.04	0.05	0.00	0.80
TiO_2	0.06	0.19	1.11	0.82	0.82	0.93	0.79	0.05
Al_2O_3	67.24	57.22	18.92	20.48	7.64	4.58	3.70	62.02
Cr_2O_3	0.77	11.67	49.01	46.52	49.86	57.77	59.76	4.57
FeO	7.03	9.96	19.51	18.67	35.92	31.63	29.64	9.14
MnO	0.00	0.05	0.17	0.12	0.55	0.50	0.48	0.17
MgO	22.34	20.27	10.10	12.34	4.47	4.83	4.81	20.94
CaO	0.04	0.04	0.11	0.05	0.07	0.01	0.00	0.07
Na_2O	0.02	0.02	0.04	0.02	0.00	0.03	0.05	0.21
K_2O	0.00	0.01	0.01	0.01	0.01	0.00	0.00	0.00
NiO	0.07	0.13	0.07	0.09	0.24	0.03	0.03	0.07
Total	97.65	99.55	99.06	99.20	99.61	100.74	99.26	98.06
Si	0.002	0.000	0.001	0.003	0.001	0.002	0.000	0.021
Ti	0.001	0.004	0.027	0.019	0.021	0.024	0.021	0.001
Al	1.993	1.750	0.714	0.755	0.312	0.188	0.155	1.873
Cr	0.015	0.239	1.241	1.151	1.367	1.593	1.674	0.093
Fe	0.148	0.216	0.522	0.488	1.041	0.923	0.878	0.196
Mn	0.000	0.001	0.005	0.003	0.016	0.015	0.014	0.004
Mg	0.837	0.784	0.482	0.575	0.231	0.251	0.254	0.800
Ca	0.001	0.001	0.004	0.002	0.003	0.000	0.000	0.002
Na	0.001	0.001	0.002	0.001	0.000	0.002	0.003	0.010
K	0.000	0.000	0.000	0.000	0.001	0.000	0.000	0.000
Ni	0.001	0.003	0.002	0.002	0.007	0.001	0.001	0.002
X_{Mg}	0.850	0.787	0.480	0.569	0.232	0.250	0.254	0.805
X_{Cr}	0.008	0.120	0.635	0.604	0.814	0.894	0.915	0.047

Notes: With sa in g P-C, spinel contacted with sarpharine included in the core of garnet pohyroblast; With chl in g P-C, spinel contacted with chlorite included in the core of porphyroblast; Incl. in g P-M, inclusion in the mantle of garnet porphyroblast; Incl. in g M-C, inclusion in the core of matrix garnet; In opx M-C, spinel included in the core of matrix orthopyroxene; In g P-R and M-R, spinel included in the rims of porphyroblastic garnet and matrix garnet; Kely. after g, spinel in the kelyphite after garnet.

(4) The fine-grained garnets included in the cores of matrix orthopyroxene (Figure 3F), clinopyroxene, and Ti-chondrodite (Figure 5B) are also compositional zoned. Their cores (Incl.-C) and rims (Incl.-R) have the same compositions as the cores and inner rims of the matrix garnets, respectively. However, their high-Cr_2O_3 rims are much thinner (30 μm) than the inner rims of matrix garnet. No retrograde rim has been detected for the garnet inclusions.

Orthopyroxene

Six textural types of orthopyroxene have been recognized. (1) The fine-grained orthopyroxene in the centre parts of polyphase inclusions, which coexists with sapphirine in the cores of garnet porphyroblasts (Figure 2C), has the highest Al (0.096–0.110 apfu) and the lowest X_{Mg} (0.90–0.91), their NiO content is in the range of 0.12–0.18 wt.%. (2) The orthopyroxene grains included in the mantles of garnet porphyroblasts and in the cores of matrix garnet have the same composition, they have higher X_{Mg} (0.93–0.95) and lower Al (0.016–0.023 apfu) than those included in the cores of porphyroblastic garnet, their NiO is in the range of 0.14–0.31 wt.%. (3) The matrix orthopyroxene grains are zoned in Al, their cores have very low Al (0.002–0.003 apfu) and the Al content increases towards their rims (0.004–0.013, Figure 7). Their MgO, FeO, and X_{Mg} maintain constant from the cores to the rims. (4) The fine orthopyroxene grains included in the rims of garnet porphyroblasts and in the rims of matrix garnet have the same compositions as the cores of matrix orthopyroxene. (5) The rounded orthopyroxene included in the fine-grained garnet in the cores of matrix orthopyroxene (Figure 3F) has the same composition as those included in the mantles of porphyroblastic garnet and those included in the cores of matrix garnet (Figures 2A and 2D). (6) The rounded orthopyroxene (opx1) included in the cores of matrix orthopyroxene (Figure 4B) has the lowest NiO content (0.02–0.05 wt.%) and high MgO (X_{Mg} = 0.93–0.94),

Table 4. Representative compositions of Ti-chondrodite and Ti-clinohumite.

Sample no.	06MW11	06MW11	06MW11	06MW11	06MW11	06MW11
Analysis no.	98	80	81	55	56	146
Mineral	Ti-chn	Ti-chn	Ti-chn	Ti-chu	Ti-chu	Ti-chu
Texture	Incl. in opx M-C	M-C	M-R near sym.	Incl. in opx M-C	M-C	M-R near sym.
SiO_2	33.44	33.76	33.04	36.28	36.14	36.85
TiO_2	8.63	8.78	9.04	4.28	4.50	3.27
Al_2O_3	0.03	0.00	0.00	0.01	0.00	0.00
Cr_2O_3	0.07	0.00	0.04	0.36	0.34	0.00
FeO	7.39	6.98	8.37	7.31	7.05	7.63
MnO	0.06	0.10	0.00	0.12	0.03	0.17
MgO	47.35	47.07	46.19	47.96	47.87	49.04
CaO	0.01	0.01	0.01	0.08	0.00	0.01
Na_2O	0.00	0.02	0.02	0.00	0.01	0.01
K_2O	0.00	0.00	0.00	0.01	0.00	0.00
NiO	0.42	0.32	0.34	0.68	0.75	0.72
F	0.97	0.74	0.85	0.66	0.44	0.80
Cl	0.00	0.00	0.00	0.01	0.00	0.00
H_2O	1.08	1.16	1.06	0.57	0.64	0.63
Total	99.44	98.94	98.96	98.32	97.78	99.13
Norm	7	7	7	13	13	13
Si	1.998	2.024	1.993	3.992	3.991	4.007
Ti	0.388	0.396	0.410	0.354	0.374	0.267
Al	0.002	0.000	0.000	0.001	0.000	0.000
Cr	0.003	0.000	0.002	0.032	0.029	0.000
Fe	0.369	0.350	0.422	0.673	0.651	0.694
Mn	0.003	0.005	0.000	0.011	0.003	0.016
Mg	4.216	4.207	4.154	7.867	7.881	7.950
Ca	0.000	0.000	0.000	0.009	0.000	0.001
Na	0.000	0.002	0.002	0.000	0.003	0.002
K	0.000	0.000	0.000	0.001	0.000	0.000
Ni	0.020	0.015	0.016	0.060	0.067	0.063
F	0.183	0.141	0.163	0.230	0.154	0.275
OH	0.429	0.463	0.427	0.416	0.472	0.457
X_{Mg}	0.920	0.923	0.908	0.921	0.924	0.920
X_F	0.092	0.070	0.081	0.115	0.077	0.138

Notes: The composition were normalized to 7 and 13 cations. All Fe is treated as FeO. H_2O was calculated on the basis of the measured F and Ti contents using the exchange vectors $Ti_xO_{2x}M_{1-x}(OH)_{2-2x}$ and $OH\text{-}F_{-1}$. $X_F = F/2$. Incl., inclusion; M-C, matrix core; M-R, matrix rim; sym., symplectite.

indicating that it is in equilibrium with the rounded olivine included in the cores of matrix orthopyroxene.

Clinopyroxene

Two textural types of clinopyroxene are recognized: (1) the medium-grained matrix clinopyroxene (Figure 3A), and (2) the fine-grained clinopyroxene included in the cores of matrix orthopyroxene (Figure 5E). Both of them have high contents of MgO (X_{Mg} = 0.93–0.94), NiO (0.15–0.22 wt.%), Cr_2O_3 (0.96–1.10 wt.%) and Na_2O (1.20–1.37 wt.%), and low content of Al_2O_3 (0.94–1.40 wt.%).

Olivine

Two textural types of olivine have been recognized. The rounded olivine included in the cores of matrix orthopyroxene has relatively lower NiO (0.20–0.42 wt.%) and X_{Mg} (0.91–0.93), whereas the olivine in the symplectite after Ti-clinohumite and Ti-chondrodite has higher X_{Mg} (0.92–0.94) and NiO content (0.52–0.98 wt.%) and detectable TiO_2 (0.12–0.47 wt.%).

Spinellide

Several textural types of spinellide have been recognized, each textural spinellide has a distinctive compositional range, and their X_{Mg}–X_{Cr} shows a negative correlation (Figure 8). (1) All the minute spinel grains coexisting with sapphirine in the cores of polyphase inclusions (with sa in g P-C, Figure 8) have the same compositions, they contain the lowest X_{Cr} (=Cr/[Cr + Al] = 0.01–0.02) and the highest X_{Mg} (0.81–0.86). (2) The fine spinel grains coexisting with chlorite and talc in the rims of polyphase inclusions (with chl in g P-C, Figure 2B) contain slightly higher X_{Cr} (0.10–0.20) and lower X_{Mg} (0.74–0.80) than those associated with sapphirine. (3) The rounded chromite included in the mantles of garnet porphyroblasts (In g P-M, Figure 2A)

Table 5. Representative composition of amphibole, formula unit based on 23 oxygen.

Sample no.	06MW11	06MW11	06MW11	06MW11	06MW11	06MW11	06MW11
Analysis no.	110	118	244	245	122	161	132
Texture	With sa in g P-C	With chl in g P-C	ged incl. in g P-C	ged incl. in g P-C	Incl. in g P-M	Incl. in g M-C	Kely.
SiO_2	46.05	47.77	45.74	43.21	43.01	42.95	41.94
TiO_2	0.84	0.12	0.08	0.04	0.06	0.08	0.24
Al_2O_3	14.68	12.96	18.83	22.31	19.38	19.49	17.19
Cr_2O_3	0.47	0.58	0.52	0.00	0.12	0.00	0.17
FeO	3.41	3.67	5.22	4.54	4.29	4.19	4.60
MnO	0.06	0.07	0.12	0.07	0.05	0.06	0.05
MgO	17.64	18.40	24.56	24.07	16.25	15.80	18.34
CaO	12.44	11.48	0.32	0.37	11.59	11.26	11.55
Na_2O	1.90	1.54	2.01	2.37	2.20	2.07	3.41
K_2O	0.21	0.08	0.00	0.01	0.15	0.18	0.04
NiO	0.15	0.11	0.04	0.00	0.11	0.06	0.07
F	0.00	0.00	0.00	0.00	0.00	0.00	0.90
Cl	0.19	0.37	0.04	0.01	0.30	0.25	0.04
Total	98.04	97.27	97.66	96.99	97.43	96.32	98.53
Si^T	6.439	6.708	6.228	5.904	6.066	6.105	5.961
Ti^C	0.088	0.013	0.008	0.004	0.007	0.008	0.025
Al^T	1.561	1.292	1.772	2.096	1.934	1.895	2.039
Al^C	0.858	0.852	1.250	1.495	1.287	1.371	0.841
Cr^C	0.052	0.064	0.056	0.000	0.013	0.000	0.019
Fe^C	0.399	0.431	0.595	0.519	0.505	0.498	0.547
Mn^C	0.007	0.009	0.014	0.008	0.006	0.007	0.006
Mg^C	3.534	3.535	3.042	2.978	3.078	3.069	3.517
Mg^B	0.143	0.317	1.943	1.925	0.337	0.279	0.370
Ca^B	1.864	1.728	0.047	0.054	1.751	1.714	1.759
Na^B	0.000	0.000	0.010	0.021	0.000	0.007	0.000
Na^A	0.515	0.418	0.522	0.605	0.602	0.563	0.939
K^A	0.038	0.014	0.000	0.001	0.026	0.033	0.007
Ni^C	0.150	0.110	0.044	0.000	0.111	0.055	0.071
F	0.000	0.000	0.000	0.000	0.000	0.000	0.405
Cl	0.045	0.089	0.009	0.002	0.071	0.059	0.009
X_{Mg}	0.902	0.899	0.893	0.904	0.871	0.871	0.877

Notes: With sa in g P-C, amphibole contacted with sarpharine included in the core of porphyroblastic garnet; With chl in g P-C, amphibole associated with chlorite included in the core of porphyroblastic garnet; ged incl. in g P-C, gedrite inclusion in the core of garnet porphyroblast; Incl. in g P-M, amphibole included in the mantle of garnet porphyroblast; Incl. in g M-C, amphibole inclusion in the core of matrix garnet; Kely., amphibole in fine-grained kelyphite after garnet.

has the same composition as those included in the cores of matrix garnet (In g M-C, Figure 3D), they have higher X_{Cr} (0.54–0.63) and lower X_{Mg} (0.45–0.57). (4) The rounded chromite included in the cores of matrix orthopyroxene (In opx M-C) has the same composition as those included in the rims of porphyroblastic garnet and matrix garnet, they have the highest X_{Cr} (0.82–0.92) and the lowest X_{Mg} (0.24–0.37). (5) The spinel in the kelyphite after garnet contains very high Al_2O_3 (60.02–61.47 wt.%) and X_{Mg} (0.80–0.81) and very low X_{Cr} (0.03–0.06).

Ti-clinohumite and Ti-chondrodite

Two textural types of Ti-clinohumite were recognized, those in the matrix and those included in the cores of matrix orthopyroxene. They are all homogeneous and have the same compositions. They have high X_{Mg} (0.91–0.93) and NiO (0.32–0.75 wt.%), low TiO_2 (3.27–4.62 wt.%) and F content (0.4–1.53 wt.%, $X_F = 0.07–0.14$).

Two textural types of Ti-chondrodite were recognized, the matrix Ti-chondrodite and those included in the cores of matrix orthopyroxene. They are also homogeneous and have the same compositions. They have similar X_{Mg} (0.91–0.93), NiO (0.40–0.75 wt.%), and F (0.54–0.80 wt.%, $X_F = 0.05–0.13$) to Ti-clinohumite but higher TiO_2 (7.75–8.87 wt.%, Ti/Si = 0.18–0.21) and lower FeO + MgO + MnO + NiO (51.80–54.90 wt.%).

Amphibole

Several textural types of amphibole were recognized, all of them have very high X_{Mg} (0.86–0.90) and NiO (0.07–0.24 wt.%). (1) The amphibole equilibrated with sapphirine in the cores of polyphase inclusions (With sa in g P-C, Figure 2) contains high TiO_2 (0.38–1.29 wt.%),

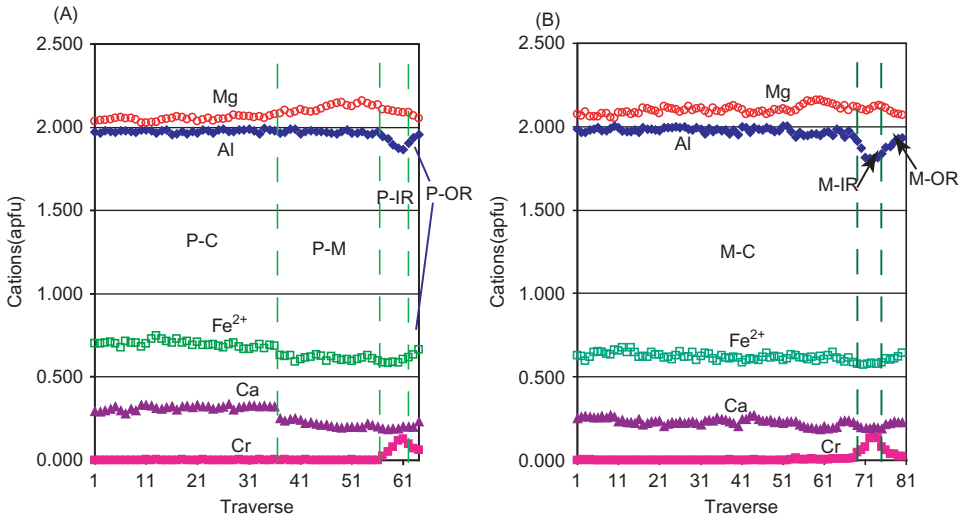

Figure 6. Zoning profiles for garnet. (A) Zoning profile of a representative porphyroblastic garnet. The path of analysis is shown in Figure 2A. P-C, core of the garnet porphyroblast; P-M, mantle of the garnet porphyroblast; P-IR, inner rim of the garnet porphyroblast; P-OR, outer rim of the garnet porphyroblast. (B) Zoning profile of a representative matrix garnet. The analytical path is shown in Figure 3D. M-C, core of the matrix garnet; M-IR, inner rim of the matrix garnet; M-OR, outer rim of the matrix garnet.

Al_2O_3 (13.83–17.84 wt.%), Na_2O (1.69–2.27 wt.%), K_2O (0.13–0.21 wt.%), and Cl (0.05–0.19 wt.%), it is pargasitic amphibole with high Tschermak component (Table 5, Figure 9). No F has been detected. (2) There are two types of amphibole in equilibrium with chlorite and talc in the rims of polyphase inclusions (With chl in g P-C, Figure 2): (a) calcium pargasitic amphibole with slightly lower Al_2O_3 (11.93–15.47 wt.%), Na_2O (1.16–1.88 wt.%), K_2O (0.07–0.15 wt.%), and TiO_2 (0.07–0.23 wt.%) and higher Cl (0.23–0.55 wt.%) than those associated with sapphirine; (b) Na-gedrite with high Al_2O_3 (18.04–22.31 wt.%) and Na_2O (1.91–2.68 wt.%), low CaO (0.31–0.50 wt.%) and TiO_2 (0.02–0.12 wt.%), and detectable Cl (0.01–0.04 wt.%). No F has been detected in these amphiboles. (3) The fine-grained pargasitic amphibole included in the mantles of porphyroblastic garnet (In g P-M) has same composition as those included in the cores of matrix garnet (In g M-C), they contain higher Al_2O_3 (19.23–19.49 wt.%), Na_2O (2.20–2.36 wt.%) and Tschermak component than those included in the cores of porphyroblastic garnet (Table 5, Figure 9). (4) The fine-grained amphibole in the kelyphite after garnet (Kely. after g) is also pargasitic amphibole with high Al_2O_3 (13.81–17.19 wt.%), Na_2O (2.44–3.41 wt.%), and F (0.75–0.93 wt.%), and low Cl (0.02–0.10 wt.%) and K_2O (0.02–0.11 wt.%).

Metamorphic evolution

The petrographical observations and mineral compositions described above indicate that the Maowu garnet orthopyroxenite experienced complex multistage metamorphism. Six metamorphic stages are classified, referred to as M_1 to M_6 in the following sections. Detailed metamorphic assemblages and textures of each stage are described below.

M_1: High-T low-P metamorphism

The earliest metamorphism (M_1) is recorded by the occurrence of a high-temperature mineral assemblage of sapphirine, high-Mg garnet, corundum, high-Al–Ti low-Cl amphibole, Al-rich orthopyroxene, and Mg–Al spinel. These minerals are limited in the centre parts of polyphase inclusions in the cores of porphyroblastic garnet (Figure 2). All these inclusions have high X_{Mg}, suggesting their ultramafic origin. Although the volume proportions of the M_1 minerals are various in various polyphase inclusions, the same mineral in different polyphase inclusions has the same composition. This character indicates that the whole rock reached chemical equilibrium during M_1 metamorphism, and the M_1 polyphase inclusions are relict fragments of the whole rock, which escaped effects by later stage metamorphism. The M_1 minerals are commonly surrounded by a group of low-temperature minerals of chlorite, talc and gedrite, and the M_1 garnet has different composition from the cores of the porphyroblastic garnet. These textural and compositional features indicate that the M_1 high-temperature minerals record a distinctive stage of metamorphism, which predates the formation of those low-temperature minerals (M_2, see later section). Therefore, the mineral assemblage of M_1 metamorphism can be constrained to be garnet + pargasitic amphibole + orthopyroxene + sapphirine + spinel. The

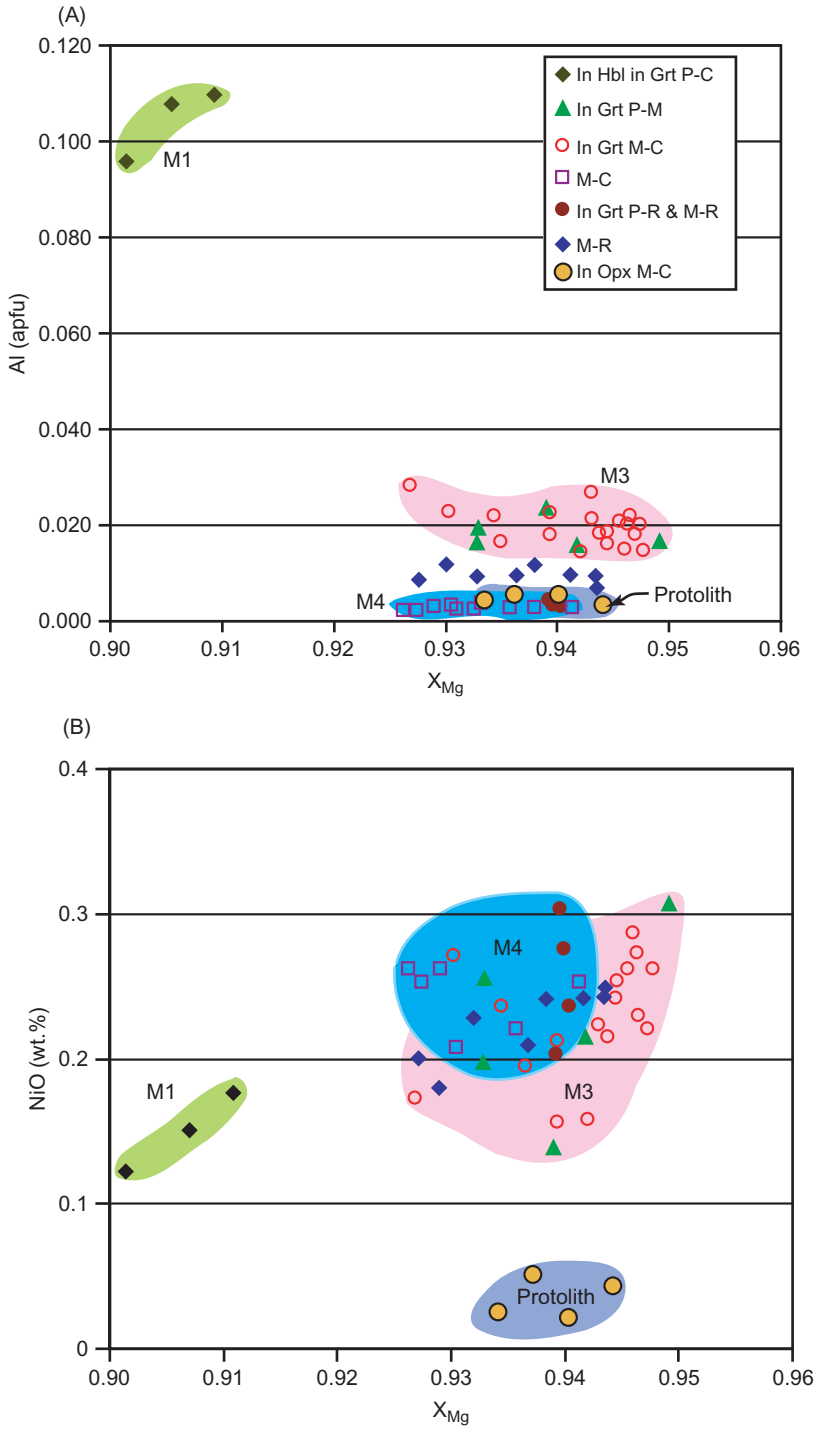

Figure 7. Chemical composition of orthopyroxene, in terms of (A) Al *versus* X_{Mg} [=Mg/(Mg + Fe)] and (B) NiO *versus* X_{Mg}. In g P-C, inclusion in core of the garnet porphyroblast; In g P-M, inclusion in mantle of the garnet porphyroblast; In g M-C, inclusion in core of the matrix garnet; M-C, core of the matrix orthopyroxene; In g P-R and M-R, inclusion in rim of porphyroblastic and matrix garnet; M-R, rim of matrix orthopyroxene; In opx M-C, inclusion in core of the matrix orthopyroxene.

stabilities of Mg–Al spinel, high-Ti amphibole, high-Al orthopyroxene, and sapphirine indicate that M_1 is a low-pressure high-temperature metamorphic stage (Klemme and O'Neill 2000; Klemme 2004).

M_2: Low-T low-P metamorphism

The second stage of metamorphism (M_2) is recorded by the occurrence of low-temperature mineral assemblage of chlorite, talc, Cr-spinel, low-Ti high-Ba–Cl amphibole,

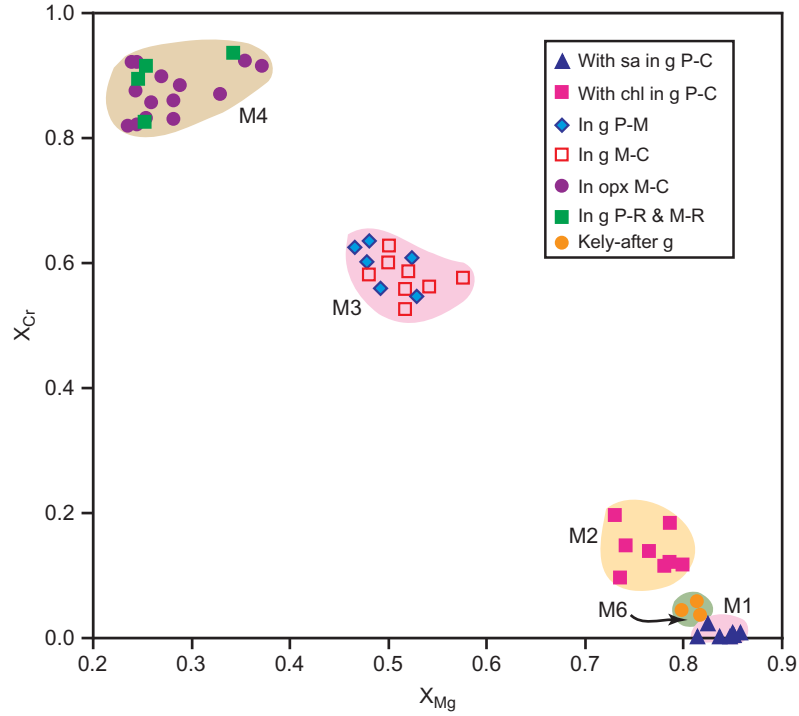

Figure 8. Diagram of X_{Mg} *versus* X_{Cr} for spinellide. With sa in g P-C, spinel contacted with sapphirine included in the core of the porphyroblastic garnet; With chl in g P-C, spinel associated with chlorite included in the core of the porphyroblastic garnet; In g P-M, spinel included in the mantle of the porphyroblastic garnet; In g M-C, spinel included in the core of the matrix garnet; In opx M-C, spinel included in the core of the matrix orthopyroxene; In g P-R and M-R, spinel included in the rims of the porphyroblastic garnet and matrix garnet; Kely. after g, spinel in the kelyphite after garnet.

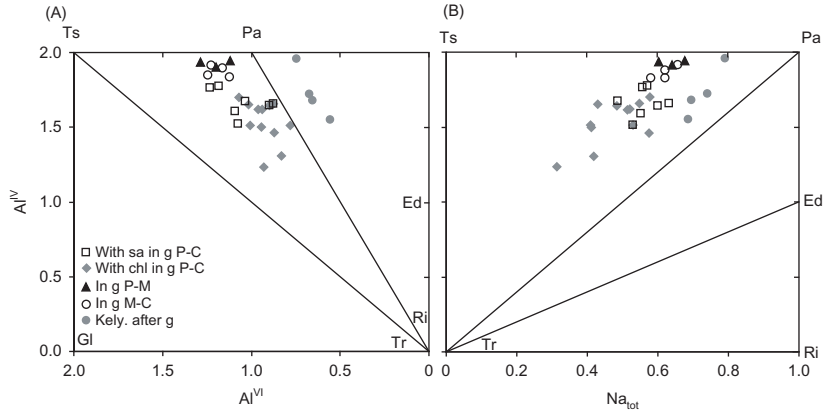

Figure 9. Diagrams of Al^{IV} *versus* Al^{VI} (A) and Al^{IV} *versus* Na (B) for clinoamphibole in the Maowu garnet orthopyroxenite. With sa in g P-C, amphibole in equilibrium with sapphirine occur in the cores of the polyphase inclusions in the cores of the porphyroblastic garnet; With chl in g P-C, amphibole in equilibrium with chlorite occur in the rims of the polyphase inclusions in the cores of the porphyroblastic garnet; In g P-M, amphibole included in the mantles of the garnet porphyroblast; In g M-C, amphibole inclusion in the cores of matrix garnet; Kely. after g, amphibole in fine-grained kelyphite after garnet.

gedrite, rutile, apatite, and Fe–Ni-rich sulphides, which occur in the rim parts of the polyphase inclusions (Figure 2). The host garnet cores, which have different composition from the M_1 garnet inclusions, are commonly in direct contact with the M_2 inclusions (Figure 2), we regard that the high-Ca–Fe cores of the porphyroblastic garnet are also formed in M_2. Therefore, the mineral assemblage of M_2 metamorphism can be constrained to be chlorite + talc + garnet + Cr spinel + Cl-rich pagasitic amphibole + gedrite + rutile + apatite. The compositions of M_2 minerals, including the high-Ca–Fe cores of the porphyroblastic garnet, all fall in narrow ranges, indicating

that M_2 minerals reached equilibrium in the whole rock. The stabilities of chlorite, talc, Cr spinel, and gedrite denote low-temperature and low-pressure conditions for M_2 metamorphism (Poli and Schmidt 2002; Fumagalli and Poli 2005; Ferri *et al*. 2009).

M_3: Low-T high-P metamorphism

The third stage of metamorphism (M_3) is characterized by the growth of the low-Ca–Cr mantles of the porphyroblastic garnet and minerals included in this zone. We have observed inclusions of low-Al orthopyroxene, chromite, pargasitic amphibole, chlorite, and rutile in the mantles of the porphyroblastic garnet, which are distinct both in assemblage and in compositions from those of M_1 and M_2 inclusions. The cores of matrix garnet has the same composition as the mantles of garnet porphyroblasts, and compositions of the fine-grained inclusions of orthopyroxene, chromite, amphibole, and chlorite in the cores of matrix garnet are also similar to those included in the mantles of garnet porphyroblasts. These features infer that the cores of the medium-grained matrix garnet and mineral inclusions are formed in the same stage (M_3) as the mantles of the garnet porphyroblasts. Therefore, the M_3 equilibrium assemblage can be constrained to be garnet + low-Al orthopyroxene + chromite + pargasitic amphibole + chlorite + rutile. The M_3 orthopyroxene has lower Al_2O_3 (0.45–0.58 wt.%) than the M_1 orthopyroxene (Figure 7A), and the M_3 chromite has higher X_{Cr} than the M_1 and M_2 ones (Figure 7B), suggesting that the M_3 minerals were formed at a higher pressure condition than M_1 and M_2. The stability of chlorite constrains M_3 to a low-temperature condition (Fumagalli and Poli 2005).

M_4: UHP metamorphism

The fourth stage of metamorphism (M_4) is characterized by the occurrence of the high-Cr inner rims of porphyroblastic garnet and matrix garnet as well as inclusions in these zones. The fine-grained orthopyroxene included in the rims of matrix garnet has the same composition as the cores of matrix orthopyroxene. These features indicate that the cores of matrix orthopyroxene are in equilibrium with the high-Cr rims of garnet. The Ti-clinohumite, Ti-chondrodite, and clinopyroxene included in the cores of the matrix orthopyroxene have the same compositions as the matrix ones, we have never observed them in the cores and mantles of the garnet porphyroblasts, indicating that they are index M_4 minerals. Compared to the M_3 low-Cr garnet, the M_4 garnet contains much higher Cr_2O_3, indicating that some chromite component had decomposed at very high-pressure conditions to form Cr-rich garnet (Klemme 2004). Such high-Cr garnet formed in the peak UHP stage was also reported in the Zhimafang garnet peridotite from the Sulu UHP terrane (Ye *et al*. 2009). The M_4 orthopyroxene contains the lowest Al_2O_3 (<0.1 wt.%) (Figure 7A), the M_4 clinopyroxene contains high jadeite and kosmochlor components, and the M_4 chromite contains the highest X_{Cr} (0.82–0.92) (Figure 8), all these compositional features suggest that M_4 metamorphism happened at UHP conditions. The absence of chlorite and pagasitic amphibole in M_4 indicates that amphibole and chlorite dehydration reactions might have taken place due to continuous increase of pressures during transition from M_3 to M_4.

M_5: Early stage retrogression

The fifth stage of metamorphism (M_5) is recorded by the breakdown of Ti-clinohumite and Ti-chondrodite to fine-grained symplectite of olivine and ilmenite (Figure 5). The breakdown reactions of the Ti-rich humites, such as Ti-chondrodite = olivine + ilmenite + fluid and Ti-clinohumite = olivine + ilmenite + fluid (Hermann *et al*. 2007), usually happened during decompression processes (Figure 12, Ulmer and Trommsdorff 1995; Trommsdorff *et al*. 2001). The Ti-chondrodite and Ti-clinohumite contain minor F (X_F = 0.07–0.15), thus the fluid equilibrated with the symplectitic olivine and ilmenite should be F-bearing.

M_6: Late stage retrogression

The lastest stage of metamorphism (M_6) is recorded by the occurrence of fine-grained kelyphite of F-rich hydrous minerals (chlorite, talc, amphibole, and phlogopite), aluminous spinel, and antigorite, which are after garnet and orthopyroxene. In some cases, the kelyphitic minerals crosscut the symplectite after Ti-clinohumite and Ti-chondrodite (Figures 5E and 5F).

P–T pseudosections and P–T estimates

In order to constrain the stability fields of each mineral assemblages and to estimate P–T conditions of each metamorphic stages, we calculated two P–T pseudosections (Figures 10 and 11) using the program of THERMOCALC 3.33 (Powell *et al*. 1998, and upgrades), the internally consistent thermodynamic data set of Holland and Powell (1998) in the NCFMASH chemical system. The bulk composition of the Maowu garnet orthopyroxenite is analysed using method of XRF in the State Key Laboratory of Lithospheric Evolution, Institute of Geology and Geophysics, Chinese Academy of Sciences. The garnet orthopyroxenite is a mafic rock (SiO_2 = 50.46 wt.%), however, it is not a typical basaltic rock. Compared to the basaltic rock, it contains higher MgO (27.81 wt.%, X_{Mg} = 0.85), and lower Fe_2O_3

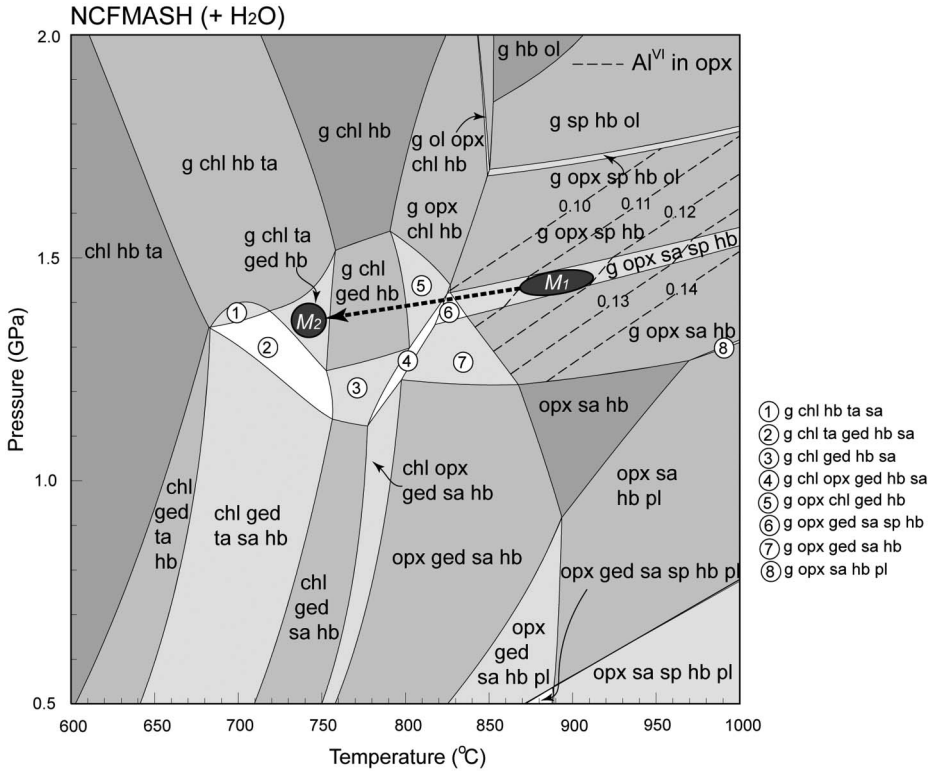

Figure 10. P–T pseudosection based on the calculated bulk composition (in mol.%) for polyphase inclusions and the host garnet cores; $SiO_2 = 42.20$, $Al_2O_3 = 13.43$, $CaO = 3.44$, $MgO = 36.30$, $FeO = 3.19$, $Na_2O = 1.43$. Al^{VI} isopleth of orthopyroxene, P–T conditions of M_1 to M_2 are also shown.

(8.44 wt.%), Al_2O_3 (10.61 wt.%, A/AFM [molecular $Al_2O_3/(Al_2O_3 + MgO + FeO)] = 0.11$), CaO (1.47 wt.%) and Na_2O (0.06 wt.%). Non-NCFMASH (Na_2O–CaO–FeO–MgO–Al_2O_3–SiO_2–H_2O) components are minor, which include TiO_2 (0.12 wt.%), P_2O_5 (0.10 wt.%), MnO (0.19 wt.%), and K_2O (0.01 wt.%). The pseudosections constructed involve garnet, orthopyroxene, clinopyroxene, olivine, hornblende, gedrite, actinolite, sapphirine, spinel, chlorite, talc, antigorite, plagioclase, quartz, and H_2O. Ti-clinohumite, Ti-chondrodite, and chromite are neglected in the pseudosection calculations, because the activity–composition models of these minerals are not available. Neglecting Cr component in the system will shift the stability of spinel to lower pressure (Klemme and O'Neill 2000; Klemme 2004). Rutile and ilmenite are very minor (<1%) in the Maowu garnet orthopyroxenite, so these two minerals are also neglected. The datafile coding of the activity–composition models is downloaded from the THERMOCALC website: http://www.metamorph.geo.uni-mainz.de/thermocalc/datafiles/index.html, with recent sapphirine model in addition (Taylor-Jones and Powell 2010). Calculated X_{Mg} and X_{Grs} isopleths for garnet, Al^{VI} isopleth for orthopyroxene are also shown.

The Maowu garnet orthopyroxenite is mainly composed of the M_3 and M_4 matrix garnet and orthopyroxene (>95 vol.%). Therefore, the bulk-rock composition of the garnet orthopyroxenite can be used to model the phase relations during the formation of matrix phases (M_3–M_4). The high-Ca–Fe cores of garnet porphyroblasts are inferred to have not been in chemical equilibrium with the matrix garnet and orthopyroxene during growth of the polyphase inclusion assemblage, as is clear from the garnet chemical composition. Thus, modelling of the expected phase equilibrium during M_1 and M_2 metamorphism would require estimating the chemically isolated volume of polyphase inclusions and the host garnet cores to obtain a new effective whole-rock composition. In order to obtain an effective bulk composition for M_1–M_2, we calculated an average composition on 30 polyphase inclusions and host garnet cores. Each bulk-rock composition was generated by integrating the modal abundance information of the phases as presented before, with the microprobe analyses (White *et al*. 2003; Wei *et al*. 2009). The modal abundance for each phase was obtained by element mapping approach.

Here, the P–T conditions of M_1 to M_4, are approached using the calculated P–T pseudosections (Figures 10 and 11), and the P–T conditions of M_5 and M_6 are estimated by the stabilities of the index minerals which are constrained by experimental works and modelling calculations.

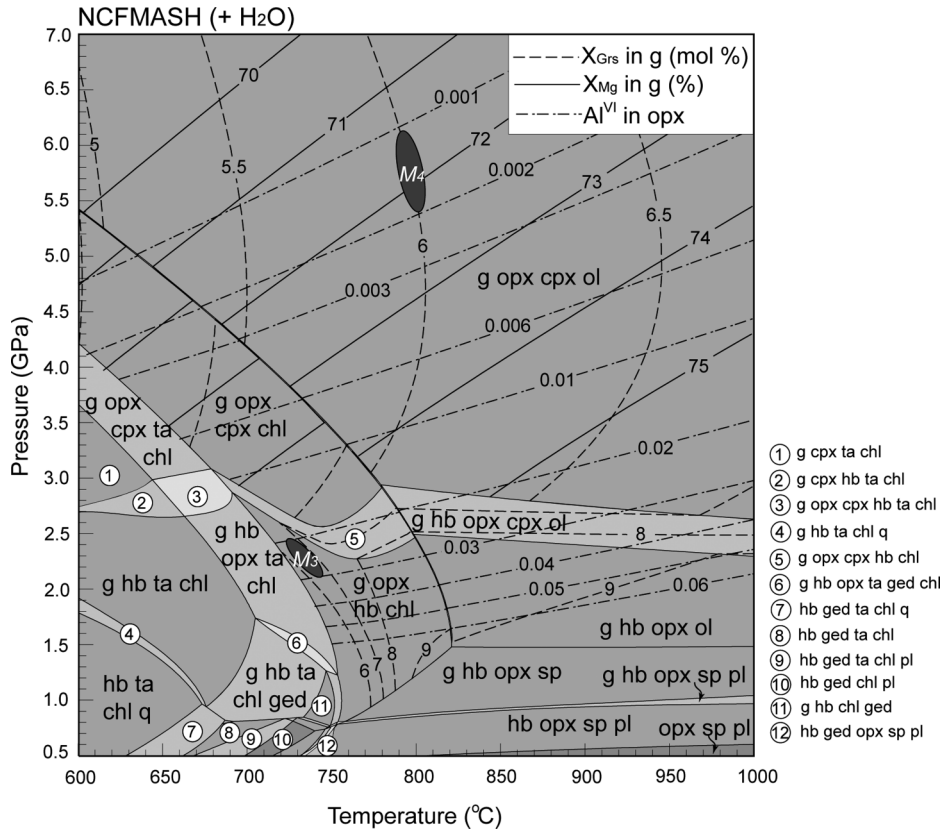

Figure 11. P–T pseudosection based on the bulk composition (in mol.%) of the Maowu garnet orthopyroxenite; SiO_2 = 46.56, Al_2O_3 = 5.83, CaO = 1.47, MgO = 38.67, FeO = 6.58, Na_2O = 0.05. X_{Mg} [=Mg/(Mg + Fe)] and X_{Grs} [=Ca/(Ca + Mg + Fe)] isopleths of garnet, Al^{VI} isopleths of orthopyroxene are also shown. P–T conditions of M_3 to M_4 are constrained based on observed mineral assemblages and mineral compositions, respectively.

M_1: High-T low-P metamorphism

Figure 10 shows the calculated P–T pseudosection using the calculated bulk composition for polyphase inclusions and host garnet cores. Our P–T pseudosection calculation shows that, even though in the silica under-saturated system, the stability P–T conditions of the M_1 mineral assemblage g + opx + sa + sp + hb are higher than ~820°C and in between 1.3–1.6 GPa. Taking into account the composition of M_1 orthopyroxene (Al^{VI} = 0.11), the Al^{VI} isopleth of orthopyroxene further constrains the P–T conditions of M_1 metamorphism at ~1.4 GPa and ~850°C. The constrained high-temperature result is in consistent with the following mineral compositions which strongly suggest that the M_1 minerals were formed at high-temperature conditions: the high Mg (X_{Mg} = 0.77) in garnet, the high Al_2O_3 content (3.6–4.1 wt.%) in M_1 orthopyroxene and the high Ti content (TiO_2: 0.38–1.29 wt.%) and high Tschermak component in M_1 amphibole. For comparison, we also calculated the M_1 P–T conditions using the g–amp (Ravna 2000) and the g–opx thermometers (Harley 1984) combined with the g–opx barometers of Nickel and Green (1985) and Brey and Kohler (1990), whose results are not affected by the water activity conditions, these calculations also give results of 835–887°C and 1.2–1.6 GPa. These calculated results are consistent with the occurrence of M_1 mineral assemblage of sapphirine + spinel that commonly occurs in high-temperature/ultrahigh-temperature silica under-saturated granulites (Horrocks 1983; Baba 2003).

M_2: Low-T low-P metamorphism

In the calculated P–T pseudosection (Figure 10), the M_2 mineral assemblage g + chl + ta + ged + hb we observed in the Maowu garnet orthopyroxenite is stable in a very narrow range (~1.4 GPa, ~750°C), which is consistent with experimental constraints of the stability of chlorite and talc (Fumagalli and Poli 2005). For comparison, the g–amp thermometer (Ravna 2000) is also used to yield the temperature conditions for M_2 at assumed pressure 1.5 GPa, based on the compositions of the cores of garnet porphyroblasts and pargasitic amphibole in the rim parts of polyphase inclusions. The g–amp thermometer (Ravna 2000) yields 693–738°C at 1.5 GPa for M_2, consistent with the THERMOCALC results. These calculated results clearly imply that the M_2 minerals were formed at lower temperature conditions than M_1 minerals.

M_3: Low-T high-P metamorphism

Figure 11 shows the calculated P–T pseudosection using the bulk-rock composition of the Maowu garnet orthopyroxenite. In the calculated P–T pseudosection, the M_3 mineral assemblage g + opx + hb + chl we observed in the Maowu garnet orthopyroxenite is stable in a very large P–T range (0.8–2.8 GPa, 700–800°C). Taking into account the X_{Grs} (0.06–0.07) of the mantles of the garnet porphyroblasts and Al^{VI} (0.02–0.03 pfu) of the orthopyroxene inclusions, P–T conditions of M_3 are further constrained at 2.1–2.5 GPa and 740–760°C. For comparison, we also calculated P–T conditions using the g–opx thermometer of Harley (1984) combined with the g–opx barometers of Nickel and Green (1985) and Brey and Kohler (1990), these calculations give results of 751–794°C and 2.4–2.7 GPa, which are consistent with the THERMOCALC calculation results.

M_4: UHP metamorphism

In the calculated P–T pseudosection (Figure 11), although olivine is expected at UHP conditions, its proportion in the UHP field of g + opx + cpx + ol is very minor (<0.03 mol.%). Therefore, although we did not observe olivine in this stage, we consider that this mineral assemblage can be regarded as the M_4 mineral assemblage g + opx + cpx that we observed in the Maowu garnet orthopyroxenite, and the isopleth behaviours in the higher variance assemblage of g + opx + cpx will be similar to those predicted in g + opx + cpx + ol. Such discrepancy of olivine between the calculated pseudosection and observation might be caused by neglecting effects of the minor Mg-rich Ti-clinohumite and Ti-chondrodite. Further, taking into account of compositions of the high-Cr inner rims of garnet porphyroblasts (X_{Grs} = 0.06, X_{Mg} = 0.72) and the cores of the matrix orthopyroxene (Al^{VI} = 0.001–0.002 pfu), P–T conditions of M_4 are constrained at 5.3–6.3 GPa and ~800°C (Figure 11). The grossular values of garnet are very sensitive to the temperatures, thus, the uncertainty from microprobe analysis will affect the result of temperatures. Here, we also calculated P–T conditions using the g–opx thermometer of Harley (1984) combined with the g–opx barometers of Nickel and Green (1985) and Brey and Kohler (1990), these calculations give results of 800–870°C and 5.7–6.5 GPa, which are consistent with the THERMOCALC calculation results.

M_5: Early stage retrogression

It is very hard to use the pseudosection to estimate the P–T conditions of M_5 due to the simplicity of the mineral assemblage and lacking of suitable activity models for Ti-chondrodite and Ti-clinohumite; however, the lack of chlorite in M_5 under fluid-saturated conditions suggest that the P–T conditions of M_5 is outside the chlorite stability field, and thus its temperature is higher than ~750°C (Fumagalli and Poli 2005). Experimental work (Trommsdorff *et al*. 2001) indicates that the presence of F will shift the stability of Ti-clinohumite to lower pressures (Figure 12). The breakdown reaction of F-bearing (X_F = 0.07–0.15) Ti-clinohumite takes place at pressures lower than 3 GPa at temperatures >750°C (Figure 12).

M_6: Late stage retrogression

The stability of antigorite constrains the temperature of M_6 to be lower than 680°C (Padron-Navarta *et al*. 2010). The decompression of garnet and orthopyroxene in this stage constrains the pressure to be lower than 2.3 GPa and the temperature to be lower than 670°C (Figure 12).

The above petrological and mineralogical studies, as well as P–T estimates, reveal that the garnet orthopyroxenite in the Maowu mafic–ultramafic body have experienced a complex tectonometamorphic history (Figure 13). Our new data indicate that the metamorphic evolution of the Maowu garnet orthopyroxenite consists of an early stage of cooling (M_1–M_2) from low-pressure, high temperature metamorphism, followed by a compression stage and HP–UHP metamorphism (M_3–M_4) and then two stages of retrogression (M_5–M_6).

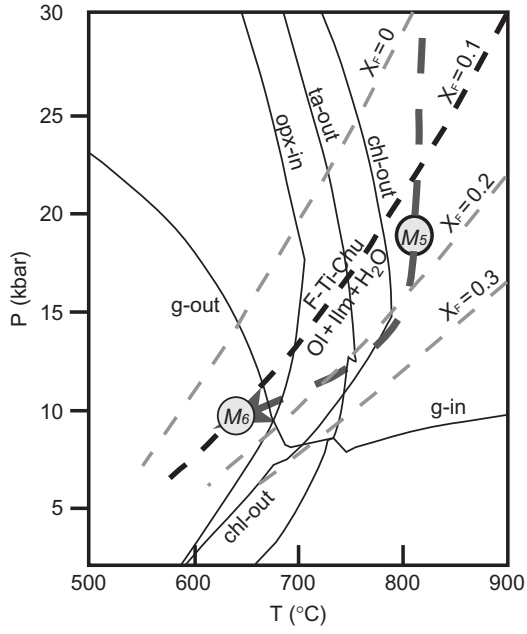

Figure 12. P–T estimations of M_5 and M_6 based on stabilities of F–Ti-clinohumite, chlorite, talc, garnet, and orthopyroxene. The stability of F–Ti-clinohumite is constructed based on experimental data of Trommsdorff *et al.* (2001). The stabilities of chlorite, talc, garnet, and orthopyroxene are constrained based on THERMOCALC calculations shown in Figure 11.

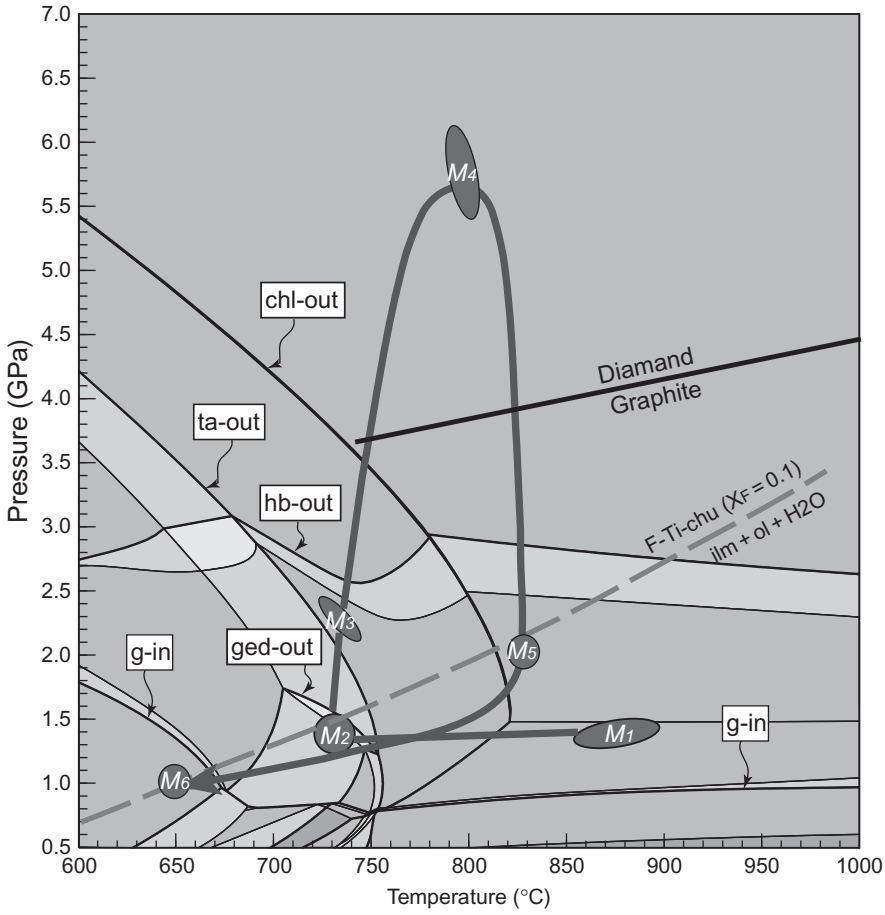

Figure 13. P–T path for the metamorphic evolution of the Maowu garnet orthopyroxenite. Numbers refer to metamorphic stages in the text. The stability of F–Ti-clinohumite ($X_F = 0.1$) is constructed based on experimental data of Trommsdorff *et al.* (2001).

Discussion and conclusions

The protolith of the Maowu garnet orthopyroxenite

The protolith of the Maowu mafic–ultramafic body has been debated for more than 20 years. Many researchers (e.g. Okay 1994; Fan *et al*. 1996; Liou and Zhang 1998; Zhang *et al*. 1998; Jahn *et al*. 2003) considered that the protolith of the Maowu mafic–ultramafic rocks was a cumulate mafic–ultramafic complex formed by fractional crystallization of a basaltic magma in the Yangtze Craton, which experienced deep subduction and UHP metamorphism in the Triassic. However, Malaspina *et al*. (2006, 2009) suggested that the Maowu garnet pyroxenites originated from mantle garnet-harzburgite that had been metasomatized at peak UHP conditions by the crust-derived silica-rich hydrous melt. Mineral textures and mineral compositions reported in this study support the point of Malaspina *et al*. (2006, 2009).

We have observed relict rounded olivine (ol1) and orthopyroxene (opx1) included in the matrix orthopyroxene (opx2) in the studied garnet orthopyroxenite (Figure 4). Such textures imply that the opx2 might be reaction product of previous peridotite and a silica-rich liquid (Malaspina *et al*. 2006). This interpretation is further supported by mineral compositions. Olivine is the main Ni-hosting mineral in peridotite, and the peridotite pyroxenes in equilibrium with olivine always contain much lower NiO content and are the main Mn-hosting minerals (Kelemen *et al.* 1998; Sobolev *et al*. 2005). Therefore, peridotite olivine commonly has high Ni content and high Ni/Mg and Fe/Mn ratios, whereas the peridotite pyroxene has relatively low Ni content and low Ni/Mg and Fe/Mn ratios (Sobolev *et al*. 2005). The ol1 has very high Ni content (0.22–0.48 wt.%) and high Ni/Mg (0.0028–0.0053) and Fe/Mn (71–188) ratios, whereas the opx1 has relatively low Ni content (0.03–0.08 wt.%) and Ni/Mg (0.0001–0.0015) and Fe/Mn (45–60) ratios (Figure 14). Their compositions are, respectively, the same as those of matrix olivine and orthopyroxene in the Maowu harzburgite and dunite, indicating that the protolith of the Maowu orthopyroxenite is harzburgite or dunite. These compositional features indicate that the relict olivine and orthopyroxene are in equilibrium and

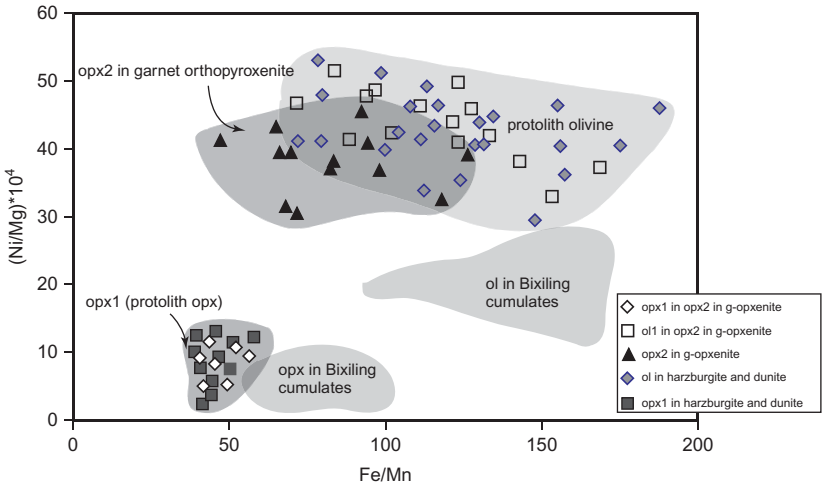

Figure 14. Diagrams of Ni/Mg *versus* Fe/Mn for olivine and orthopyroxene in the Maowu mafic–ultramafic rocks.

are relict peridotite minerals. All of the opx2 grains in the Maowu garnet orthopyroxenite have quite different compositions from the opx1, they have relatively high Ni content (0.20–0.37 wt.%), high X_{Mg} (0.93–0.95), and high Ni/Mg (0.0024–0.0048) and Fe/Mn (45–140) ratios, which are similar to those of the ol1 and the olivine in the harzburgite and dunite (Figure 14). Chemical features of the Maowu matrix orthopyroxene are also quite different from those in typical cumulate complex (e.g. Bixiling cumulate, Figure 14). These compositional features indicate that the opx2 is not fractional crystallization product, but formed by metasomatic interaction between previous olivine and silica-rich liquid, and thus inherited the compositional features of previous olivine.

Geodynamic scenario for the Maowu garnet orthopyroxenite

Our new data clearly indicate that the Maowu garnet orthopyroxenite underwent isobaric cooling from M_1 (~1.4 GPa, ~850°C) to M_2 (1.3–1.5 GPa, 720–750°C) where the polyphase inclusions were formed, and subsequently suffered HP and UHP metapmorphism (M_3–M_4), followed by late stage retrogression (M_5–M_6). The major differences between the previously published data (Okay 1994; Liou and Zhang 1998; Zhang *et al*. 2000) and our estimation are: (1) the P–T conditions for the formation of polyphase inclusions and (2) the existence of the isobaric cooling history represented by the precursor two-stage growth of polyphase inclusion minerals before the subsequent HP and UHP metapmorphism. Similar P–T paths have been reported commonly from mantle wedge peridotites, such as the Ulten peridotite in Italy (Nimis and Morten 2000; Scambelluri *et al*. 2006; Sapienza *et al*. 2009), the Zhimafang peridotite in the Sulu UHP terrane (Ye *et al*. 2009), and the Bardane websterite in the Western Gneiss Region, Norway (Spengler *et al*. 2006; Scambelluri *et al*. 2008, 2010). Further, considering the mantle harzburgite or dunite protolith nature, we suggest that the Maowu garnet orthopyroxenite probably records the metamorphism of mantle wedge process. Nimis and Morten (2000), Scambelluri *et al*. (2006), and Ye *et al*. (2009) proposed that the initial low-P high-T regime (corresponding to our M_1) reflects a shallow hot mantle wedge environment above the subduction slab, whereas the later low-P low-T regime (corresponding to our M_2) reflects a shallow cold mantle wedge corner. This transformation was probably caused by the corner-flow convection in the mantle wedge above the subduction slab (Nimis and Morten 2000; Martinez and Taylor 2002; Kelemen *et al*. 2003; Curri and Hyndman 2006; Scambelluri *et al*. 2006, 2010; Ye *et al*. 2009), which is consistent with the isobaric cooling process from M_1 to M_2 in our investigated sample. Alternatively, such a decrease in temperature may be also caused by emplacement of the peridotite into colder subducted crust, accomplished by the density contrast between the overlying mantle wedge and the underlying subducted crust (Brueckner 1998; Medaris *et al*. 2005). In both scenarios, the Maowu garnet orthopyroxenite would have been subducted to higher pressure conditions, either by downwards mantle flow (Martinez and Taylor 2002; Kelemen *et al*. 2003; Curri and Hyndman 2006; Scambelluri *et al*. 2006; Ye *et al*. 2009) or by subduction of the host crustal slab (Brueckner 1998; Brueckner and Medaris 2000), and suffered HP (M_3) and UHP (M_4) metamorphism. However, the P–T path from M_2 to M_4 is nearly isothermal compressional, and the temperatures do not show significant increase during the compression (Figure 13). This P–T path is different from the prograde P–T path of the UHP eclogite in the country gneisses, which shows increasing of temperature during the compression (Carswell *et al*. 1997). Additionally, the prograde P–T path of the mantle-derived peridotite emplaced into the cold oceanic crust prior to the subduction also shows increasing

of temperature during the compression (Yang and Powell 2008). Therefore, the Maowu garnet orthopyroxenite and the country UHP crustal rocks may not share the similar metamorphic evolution during the subduction process, we suggest that the Maowu garnet orthopyroxenite was still in the mantle wedge, and was not entrapped by the subducted continental crust (Scambelluri *et al*. 2006; Ye *et al*. 2009). Therefore, we prefer the first mechanism of mantle wedge corner-flow and downwards flow to form this type P–T path.

The retrograde P–T path from M_4 UHP metamorphism to M_5 and M_6 retrogression stages demonstrates that the Maowu garnet orthopyroxenite exhumed to the crustal level. This decompressional P–T path is similar to that of the UHP eclogite in the country gneiss (Carswell *et al*. 1997; Rolfo *et al*. 2004). We suggest that the Maowu garnet orthopyroxenite was dragged by the exhumed continental crust from the overlying mantle wedge. The formation of F-rich hydrous phases including phlogopite, amphibole, talc, chlorite, and antigorite in M_6 indicates that the garnet orthopyroxenite was metasomatized again during this exhumation process. Because the garnet orthopyroxenite may not contain sufficient K_2O, Na_2O, F, and H_2O to form phlogopite and pargasitic amphibole in the kelyphite, the formation of these hydrous phases requires substantial additions of mobile elements imported into the garnet orthopyroxenite. We consider that the K_2O, Na_2O, and F are concentrated in the metasomatic fluid or melt derived from the country gneiss.

Acknowledgements

This work was supported by the National Basic Research Programme of China (973 Programme 2009CB825001) and the National Science Foundation of China (No. 40902023, 41090371, 40922150, 41023009). Drs Q. Mao and Y. G. Ma are thanked for their help in electron microprobe analysis. This work benefited from discussions with Dr N. Malaspina, Professor J. Hermann, and Professor C. J. Wei.

Mineral abbreviations

g, garnet; opx, orthopyroxene; ol, olivine; hb, bornblende; ged, gedrite; act, actinolite; sa, sapphirine; crn, corundum; sp, spinel; chl, chlorite; ta, talc; atg, antigorite; ap, apatite; pl, plagioclase; q, quartz; ru, rutile; ilm, ilmenite.

References

Baba, S., 2003, Two stages of sapphirine formation during prograde and retrograde metamorphism in Palaeoproterozoic Lewisian Complex in South Harris, NW Scotland: Journal of Petrology, v. 44, p. 329–354.

Brey, G.P., and Kohler, T., 1990, Geothermobarometry in four-phase lherzolites II. New thermobarometers, and practical assessment of existing thermobarometers: Journal of Petrology, v. 31, p. 1353–1378.

Brueckner, H.K., 1998, A sinking intrusion model for the introduction of garnet-bearing peridotites into continental collision orogens: Geology, v. 26, p. 631–634.

Brueckner, H.K., and Medaris, L.G., 2000, A general model for the intrusion and evolution of 'mantle' garnet peridotites in high-pressure and ultra-high-pressure metamorphic terranes: Journal of Metamorphic Geology, v. 18, p. 123–133.

Carswell, D.A., O'Brien, P.J., Wilson, R.N., and Zhai, M., 1997, Thermobarometry of phengite-bearing eclogites in the Dabie Mountains of central China: Journal of Metamorphic Geology, v. 15, p. 239–252.

Curri, C.A., and Hyndman, R.D., 2006, The thermal structure of subduction zone back arcs: Journal of Geophysical Research, v. 111, p. 1–22.

Fan, Q., Liu, R., Ma, B., Zhao, D., and Zhang, Q., 1996, The protolith and ultrahigh-pressure metamorphism of Maowu mafic–ultramafic rock block in Dabieshan Mountains: Acta Petrologica Sinica, v. 12, p. 29–47 (in Chinese with English abstract).

Ferri, F., Poli, S., and Vielzeuf, D., 2009, An experimental determination of the effect of bulk composition on phase relationships in metasediments at near-solidus conditions: Journal of Petrology, v. 50, p. 909–931.

Fumagalli, P., and Poli, S., 2005, Experimentally determined phase relations in hydrous peridotite to 6.5 GPa and their consequences on the dynamics of subduction zones: Journal of Petrology, v. 46, p. 555–578.

Harley, S.L., 1984, An experimental study of the partitioning of Fe and Mg between garnet and orthopyroxene: Contributions to Mineralogy and Petrology, v. 86, p. 353–373.

Hermann, J., Gerald, J.D.F., Malaspina, N., Berry, A.J., and Scambelluri, M., 2007, OH-bearing planar defects in olivine produced by the breakdown of Ti-rich humite minerals from Dabie Shan (China): Contributions to Mineralogy and Petrology, v. 153, p. 417–428.

Holland, T.J.B., and Powell, R., 1998, An internally consistent thermodynamic data set for phase of petrological interest: Journal of Metamorphic Geology, v. 16, p. 309–343.

Horrocks, P.C., 1983, A corundum and sapphirine paragenesis from the Limpopo Mobile Belt, southern Africa: Journal of Metamorphic Geology, v. 1, p. 13–23.

Jahn, B.M., Fan, Q.C., Yang, J.J., and Henin, O., 2003, Petrogenesis of the Maowu pyroxenite–eclogite body from the UHP metamorphic terrane of Dabieshan: Chemical and isotopic constraints: Lithos, v. 70, p. 243–267.

Kelemen, P.B., Hart, S.R., and Bernstein, S., 1998, Silica enrichment in the continental upper mantle via melt-rock reaction: Earth and Planetary Science Letters, v. 164, p. 387–406.

Kelemen, P.B., Rilling, J.L., Parmentier, E.M., Mehl, L., and Hacker, B.R., 2003, Thermal Structure due to solid-state flow in the mantle wedge beneath arcs, *in* Eiler, J., ed., Inside the subduction factory, Geophysical monograph, Volume 138: Washington, D.C., AGU, 293–311.

Klemme, S., 2004, The influence of Cr on the garnet–spinel transition in the Earth's mantle: Experiments in system MgO–Cr_2O_3–SiO_2 and thermodynamic modeling: Lithos, v. 77, p. 639–646.

Klemme, S., and O'Neill, H., 2000, The near-solidus transition from garnet lherzolite to spinel lherzolite: Contributions to Mineralogy and Petrology, v. 138, p. 237–248.

Li, S.G., Jagoutz, E., Chen, Y.Z., and Li, Q.L., 2000, Sm–Nd and Rb–Sr isotopic chronology and cooling history of ultrahigh pressure metamorphic rocks and their country rocks at Shuanghe in the Dabie Mountains, Central China: Geochimica et Cosmochimica Acta, v. 64, p. 1077–1093.

Liou, J.G., and Zhang, R.Y., 1998, Petrogenesis of an ultrahigh-pressure garnet-bearing ultramafic body from Maowu, Dabie Mountains, eastern-central China: The Island Arc, v. 7, p. 115–134.

Liu, D.Y., Jian, P., Kroner, A., and Xu, S.T., 2006, Dating of prograde metamorphic events deciphered from episodic zircon growth in rocks of the Dabie–Sulu UHP complex, China: Earth and Planetary Science letters, v. 250, p. 650–666.

Malaspina, N., Hermann, J., and Scambelluri, M., 2009, Fluid/mineral interaction in UHP garnet peridotite: Lithos, v. 107, p. 38–52.

Malaspina, N., Hermann, J., Scambelluri, M., and Compagnoni, R., 2006, Polyphase inclusions in garner-orthopyroxenite (Dabie Shan, China) as monitors for metasomatism and fluid-related trace element transfer in subduction zone peridotite: Earth and Planetary Science Letters, v. 249, p. 173–187.

Martinez, F., and Taylor, B., 2002, Mantle wedge control on back-arc crustal accretion: Nature, v. 416, p. 417–420.

Medaris, L.G., Wang, H., Jelinek, E., Mihaljevic, M., and Jakes, P., 2005, Characteristics and origins of diverse Variscan peridotites in the Gfohl Nappe, Bohemian Massif, Czech Republic: Lithos, v. 82, p. 1–23.

Menzies, M.A., Vannucci, R., and Bodinier, J.L., 2001, Orogenic lherzolites and mantle processes: Editorial: Journal of Petrology, v. 42, p. 3–4.

Nickel, K.G., and Green, D.H., 1985, Empirical geothermobarometry for garnet peridotites and implications for the nature of lithosphere, kimberlites and diamonds: Earth and Planetary Science Letters, v. 73, p. 158–170.

Nimis, P., and Morten, L., 2000, P–T evolution of 'crustal' peridotites and included pyroxenites from Nonsberg area (Upper Austroalpine), NE Italy: From the wedge to the slab: Journal of Geodynamics, v. 30, p. 93–115.

Okay, A.I., 1994, Sapphirine and Ti-clinohumite in ultrahigh-pressure garnet-pyroxenite and eclogite from Dabie Shan, China: Contributions to Mineralogy and Petrology, v. 116, p. 145–155.

Padron-Navarta, J.A., Hermann, J., Garrido, C.J., Sanchez-Vizcaino, V.L., and Gomez-Pugnaire, M.T., 2010, An experimental investigation of antigorite dehydration in natural silica-enriched serpentinite: Contributions to Mineralogy and Petrology, v. 159, p. 25–42.

Poli, S., and Schmidt, M.W., 2002, Petrology of subducted slabs: Annual Review of Earth and Planetary Sciences, v. 30, p. 207–235.

Powell, R., Holland, T.J.B., and Worley, B., 1998, Calculating phase diagrams involving solid solutions via nonlinear equations, with examples using THERMOCALC: Journal of Metamorphic Geology, v. 16, p. 577–588.

Ravna, E.L., 2000, Distribution of Fe^{2+} and Mg between coexisting garnet and hornblende in synthetic and natural systems: An empirical calibration of the garnet-hornblende Fe-Mg geothermometer: Lithos, v. 53, p. 265–277.

Rolfo, F., Compagnoni, R., Wu, W.P., and Xu, S.T., 2004, A coherent lithostratigraphic unit in the coesite-eclogite complex of Dabie Shan, China: Geologic and petrologic evidence: Lithos, v. 73, p. 71–94.

Sapienza, G.T., Scambelluri, M., and Braga, R., 2009, Dolomite-bearing orogenic garnet peridotites witness fluid-mediated carbon recycling in a mantle wedge (Ulten Zone, Eastern Alps, Italy): Contributions to Mineralogy and Petrology, v. 158, p. 401–420.

Scambelluri, M., Herman, L.M., Roemund, V., and Pettke, T., 2010, Mantle wedge peridotites: Fossil reservoirs of deep subduction zone processes: Inferences from high and ultrahigh-pressure rocks from Bardane (Western Norway) and Ulten (Italian Alps): Lithos, v. 120, p. 186–201.

Scambelluri, M., Hermann, J., Morten, L., and Rampone, E., 2006, Melt-versus fluid-induced metasomatism in spinel to garnet wedge peridotites (Ulten Zone, Eastern Italian Alps): Clues from trace element and Li abundances: Contributions to Mineralogy and Petrology, v. 151, p. 372–394.

Scambelluri, M., Pettke, T., and Can Roemund, H.L.M., 2008, Majoritic garnets monitor deep subduction fluid flow and mantle dynamics: Geology, v. 36, p. 59–62.

Sobolev, A.V., Hofmann, A.W., Sobolev, S.V., and Nikogosian, I.K., 2005, An olivine-free mantle source of Hawaiian shield basalts: Nature, v. 434, p. 590–597.

Spengler, D., Van Roemund, H.L.M., Drury, M.R., Ottolini, L., Mason, P.D., and Davies, G.R., 2006, Deep origin and hot melting of an Archean orogenic peridotite massif in Norway: Nature, v. 440, p. 913–917.

Taylor-Jones, K., and Powell, R., 2010, The stability of sapphirine + quartz: Calculated phase equilibria in FeO–MgO–Al_2O_3–SiO_2–TiO_2–O: Journal of Metamorphic Geology, v. 28, p. 615–633.

Trommsdorff, V., Risold, A.C., Reusser, E., Connolly, J.A., and Ulmer, P., 2001, Titanian clinohumite: Ilmenite rod inclusions and phase relations (abstract), Central Alps, paper presented at Workshop on Fluid/Slab/Mantle Interactions and UHP Minerals, Waseda University, Tokyo, p. 84.

Ulmer, P., and Trommsdorff, V., 1995, Serpentine stability to mantle depths and subduction-related magmatism: Science, v. 268, p. 858–861.

Wei, C.J., Yang, Y., Su, X.L., Song, S.G., and Zhang, L.F., 2009, Metamorphic evolution of low-T eclogite from the North Qilian orogen, NW China: Evidence from petrology and calculated phase equilibria in the system NCKFMASHO: Journal of Metamorphic Geology, v. 27, p. 55–70.

White, R.W., Powell, R., and Clarke, G.L., 2003, Prograde metamorphic assemblage evolution during partial melting of metasedimentary rocks at low pressures: Migmatites from Mt Stafford, Central Australia: Journal of Petrology, v. 44, p. 1937–1960.

Yang, J.J., and Jahn, B.M., 2000, Deep subduction of mantle-derived garnet peridotites from the Su-Lu UHP metamorphic terrane in China: Journal of Metamorphic Geology, v. 18, p. 167–180.

Yang, J.J., and Powell, R., 2008, Ultrahigh-pressure garnet peridotites from the devolatilization of sea-floor hydrated ultramafic rocks: Journal of Metamorphic Geology, v. 26, p. 695–716.

Ye, K., Song, Y.R., Chen, Y., Xu, H.J., Liu, J.B., and Sun, M., 2009, Multistage metamorphism of orogenic garnet-lherzolite from Zhimafang, Sulu UHP terrane, eastern China: Implications for mantle wedge convection during progressive oceanic and continental subduction: Lithos, v. 109, p. 155–175.

Zhang, R.Y., Liou, J.G., Yang, J.S., and Yui, T.F., 2000, Petrochemical constraints for dual of garnet peridotites from the Dabie–Sulu UHP terrane, eastern-central China: Journal of Metamorphic Geology, v. 18, p. 149–166.

Zhang, R.Y., Rumble, D., Liou, J.G., and Wang, Q.C., 1998, Low $\delta^{18}O$, ultrahigh-P garnet-bearing mafic and ultramafic rocks from Dabie Shan: Chemical Geology, v. 150, p. 161–170.

Zhang, R.Y., Shu, J.F., Mao, H.K., and Liou, J.G., 1999, Magnetite lamellae in olivine and clinohumite from Dabie UHP ultramafic rocks, central China: American Mineralogist, v. 84, p. 564–569.

Zheng, Y.F., Zhao, Z.F., Wu, Y.B., Zhang, S.B., Liu, X.M., and Wu, F.Y., 2006, Zircon U–Pb age, Hf and O isotope constraints on protolith origin of ultrahigh-pressure eclogite and gneiss in the Dabie orogen: Chemical Geology, v. 231, p. 135–158.